AD-A043 257 HARRY DIAMOND LABS ADELPHI MD F/G 20/3
THE EXPERIMENTAL DETERMINATION OF THE ELECTRIC FIELDS SURROUNDI--ETC(U)
JUL 77 N D WILKIN

UNCLASSIFIED HDL-TM-77-5 NL

| OF |
AD
A043 257

END
DATE
FILMED
9-77
DDC

HDL-TM-77-5

The Experimental Determination of the Electric Fields Surrounding a Model Aircraft

July 1977

U.S. Army Materiel Development
and Readiness Command
HARRY DIAMOND LABORATORIES
Adelphi, Maryland 20783

The findings in this report are not to be construed as an official Department of the Army position unless so designated by other authorized documents.

Citation of manufacturers' or trade names does not constitute an official indorsement or approval of the use thereof.

Destroy this report when it is no longer needed. Do not return it to the originator.

UNCLASSIFIED

SECURITY CLASSIFICATION OF THIS PAGE (When Data Entered)

REPORT DOCUMENTATION PAGE

READ INSTRUCTIONS BEFORE COMPLETING FORM

1. REPORT NUMBER: HDL-TM-77-5	2. GOVT ACCESSION NO.
3. RECIPIENT'S CATALOG NUMBER	
4. TITLE (and Subtitle): The Experimental Determination of the Electric Fields Surrounding a Model Aircraft.	5. TYPE OF REPORT & PERIOD COVERED: Technical Memorandum
6. PERFORMING ORG. REPORT NUMBER	
7. AUTHOR(s): Neil D. Wilkin	8. CONTRACT OR GRANT NUMBER(s)
9. PERFORMING ORGANIZATION NAME AND ADDRESS: Harry Diamond Laboratories, 2800 Powder Mill Road, Adelphi, MD 20783	10. PROGRAM ELEMENT, PROJECT, TASK AREA & WORK UNIT NUMBERS: Prog. Elem: 6.26.16.A; DA: 1W362616AH77
11. CONTROLLING OFFICE NAME AND ADDRESS: U.S. Army Materiel Development and Readiness Command, Alexandria, VA 22333	12. REPORT DATE: July 1977
	13. NUMBER OF PAGES: 59
14. MONITORING AGENCY NAME & ADDRESS (if different from Controlling Office): 52 p.	15. SECURITY CLASS. (of this report): UNCLASSIFIED
	15a. DECLASSIFICATION/DOWNGRADING SCHEDULE

16. DISTRIBUTION STATEMENT (of this Report)

Approved for public release; distribution unlimited.

17. DISTRIBUTION STATEMENT (of the abstract entered in Block 20, if different from Report)

18. SUPPLEMENTARY NOTES

HDL Project: A77613

DRCMS Code: 662616.11.H7700

19. KEY WORDS (Continue on reverse side if necessary and identify by block number)

Electrostatic
Fuze
Electric field

20. ABSTRACT (Continue on reverse side if necessary and identify by block number)

All aircraft collects electrostatic charges during flight, and use of the resultant electric fields has been proposed to initiate fuzing of antiaircraft projectiles. Plots of the resultant fields close to full-scale aircraft are difficult to obtain. An electrolytic tank may be used to measure these fields by using scaled models. Plots were made of the equipotential surfaces about an F4-J scaled aircraft and of potential differences (measure of po-

DD FORM 1 JAN 73 1473 EDITION OF 1 NOV 65 IS OBSOLETE

UNCLASSIFIED

SECURITY CLASSIFICATION OF THIS PAGE (When Data Entered)

tential gradient) between probes on prescribed trajectories past the scaled model. These data are presented in this report and can be used to estimate fuzing performance.

CONTENTS

APPENDICES

FIGURES

1. INTRODUCTION

A large amount of electrostatic charge collects on aircraft while the aircraft is in flight.[1-9,*] Aircraft manufacturers expend much effort to reduce this charge to acceptable levels, but a substantial charge remains.[10,11] This charge produces an electric field about the aircraft, and use of the resultant electric fields has been proposed to initiate fuzing of antiaircraft projectiles.[12,13] Several fuze proposals have been suggested. Two such systems are an ac electrostatic system[14] and an induction inversion fuze (IIF) system.[15,16] A related system is the dc capacitance fuze system.[17,18]

The ac electrostatic system takes advantage of the projectile spin rate by mounting probes transversely on the projectile to provide an ac signal. This ac signal reaches a maximum value at the point of closest approach and requires only a threshold device, set for an adequate level, to initiate the fuze. The ac system cannot differentiate between a miss trajectory and a collision trajectory.

The dc capacitance system detects a change in capacitance between two probes mounted on the fuze as the fuze approaches the target. This fuze requires either a collision trajectory or a near miss to cause the fuze to function.

The IIF system employs a pair of circumferential probes separated longitudinally along the projectile, resulting in no ac signal due to projectile spin. Instead, the resulting signal is a quasi-dc voltage, and the rate of change of the voltage is a function of the relative velocity between the target and the fuze. For a point source target, two peaks of opposite polarity occur during a miss trajectory with a single zero crossing located between them at the point of closest approach (PCA). During a collision trajectory, the IIF signal only increases, but never produces a zero crossing. This difference in signal character permits design of a system which would initiate the fuze at the (PCA) on miss trajectories and upon impact for a collision trajectory.

This report describes data obtained in an electrolytic tank for use in designing an IIF system. Some of the data presented are applicable to the ac system as well. These data were obtained by using a scale-model F4-J aircraft. Both equipotential and potential difference† data were obtained. Data are presented also to show the validity of electrolytic tank measurements.

---

*References in the Literature Cited section (p. 13) reflect the computer search for what had been done to validate further experimentation and to aim its direction.

†In this report, a "potential difference" is the voltage difference between two specified points, and a "potential" is a voltage difference between one specified point and infinity.

2. ELECTROLYTIC TANK

Electric-field measurements are very difficult to perform on full-scale aircraft. Valid analog field measurements[19-23] are feasible employing an electrolytic tank and scale-model aircraft. The field measurements described here were obtained by using current as the analog of the full-scale electric field. The current flows between the metalized surface of the scale-model aircraft and the stainless-steel wire basket lining the tank (fig. 1). The electrolyte, which acts as a bulk resistor, is probed to determine the electric-field configuration.

The electrolytic tank, used in acquiring the data described in this report, was assembled by using a wooden packing crate approximately 2 × 3 × 2 ft (0.61 × 0.91 × 0.61 m). The crate was lined with 1/32-in. (9.5-mm) aluminum sheets to increase the wall strength and provide electrical shielding. The crate was reinforced with steel bands to increase its strength. Two layers of large polyethylene sheeting (12 × 12 ft--3.66 × 3.66 m) were arranged in the crate to form a watertight tank. The tank was then filled with ordinary tap water,

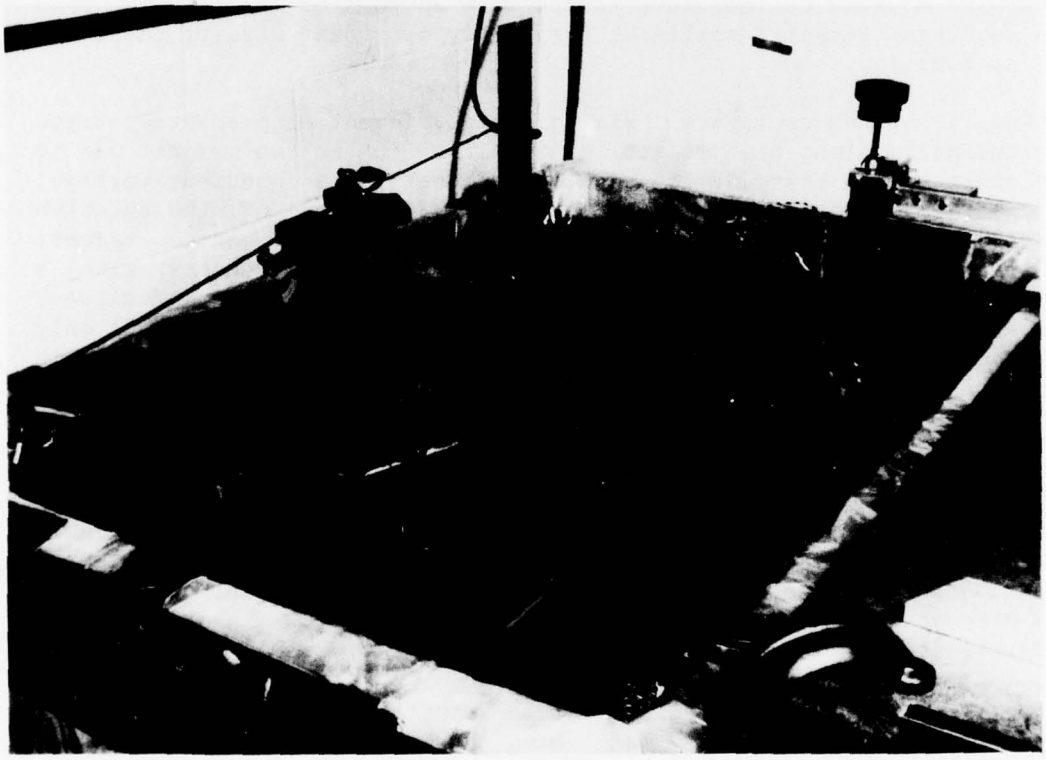

Figure 1. Electrolytic tank assembly.

which served as the electrolyte. The water was filtered continuously with an aquarium type of filter and pump assembly to remove dirt and other foreign material.

A stainless-steel basket, constructed of wire cloth on a steel frame, was placed in the electrolytic tank. This basket was constructed so the maximum distance between the model under test and the basket was obtained. The greater the separation between the basket and the model, the less the disturbance to the electric-field analog currents in the vicinity of the model.

The accuracy of the electrolytic tank simulation of full-scale electric fields was checked in two ways. The equipotential line contours were plotted about a sphere placed in the tank, and the data were compared to theoretical contours.

3. MEASURING APPARATUS

Simulation of electric fields in an electrolytic tank is best achieved by using ac measurement techniques. Direct-current measurements are difficult because of contact potential problems and because high-stability dc amplifiers are required. The test frequency of 1040 Hz was chosen, since narrow-band amplifiers were available at this frequency.

Two different measurement systems were assembled (fig. 2, 3). One system permits measurement of equipotential lines, and the other system permits potential difference plots to be determined. These systems were set up by using laboratory equipment with probes which were assembled at the Harry Diamond Laboratories (HDL) specifically for use in the electrolytic tank.

Each probe consisted of a small-diameter glass tube. Platinum wires were threaded through the tube, and the glass was sealed around the wires. For equipotential probes, a single wire was sealed in the tube, and the wire was melted to a minute-diameter ball. The potential difference probe consisted of two wires sealed in a small-diameter glass tube with their ends protruding and formed to simulate the length of a 1/48-scale, 60-mm shell, divided at the nose-body interface.

These probes were then mounted on an x-y-z carriage which accurately positioned the probe in the electrolytic tank (fig. 4). The z direction permitted various probe depths to be preset, and then the probe could be moved in the x-y directions.

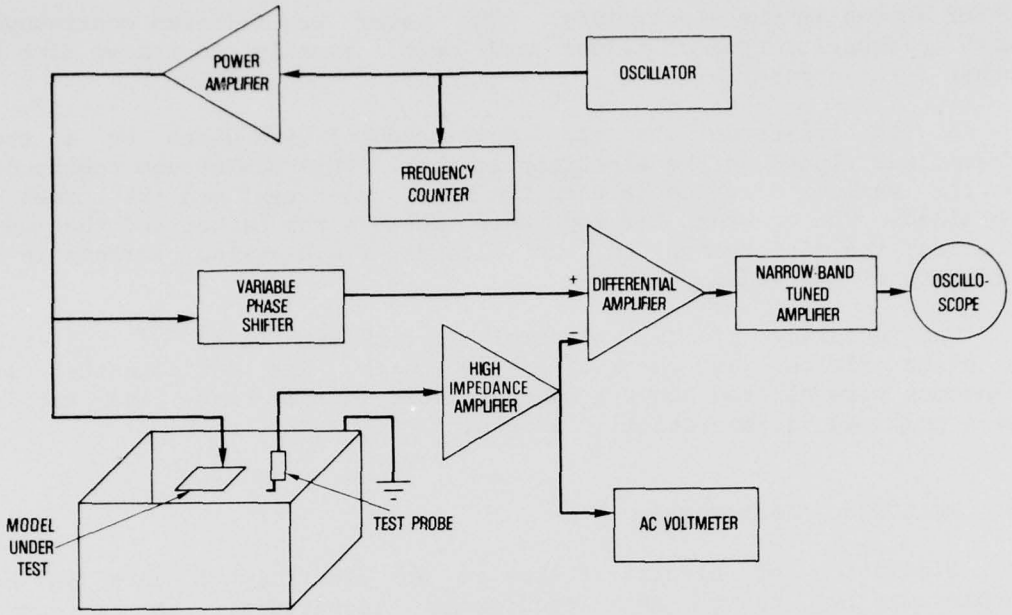

Figure 2. Functional diagram of equipotential measurement system.

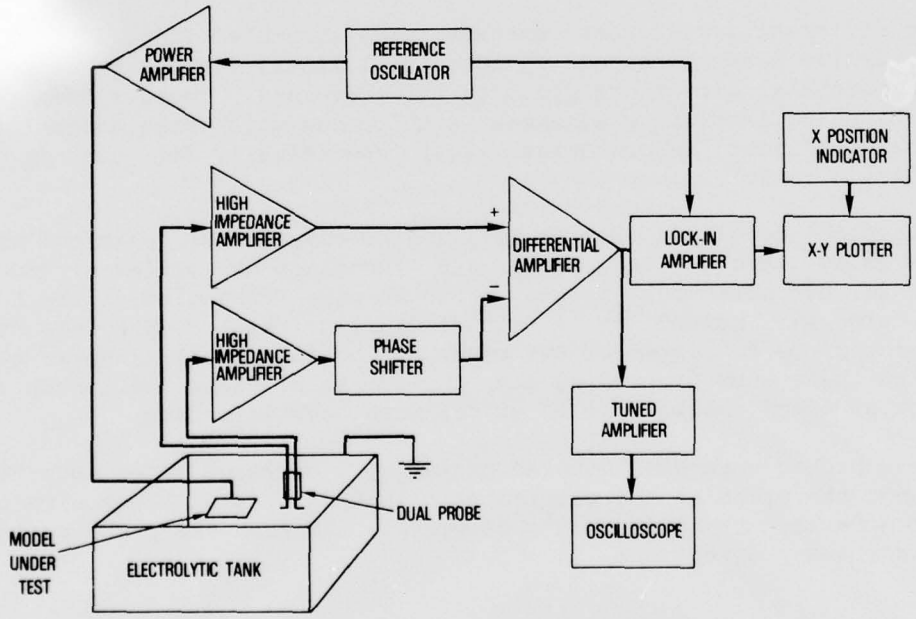

Figure 3. Functional diagram of dual-probe system.

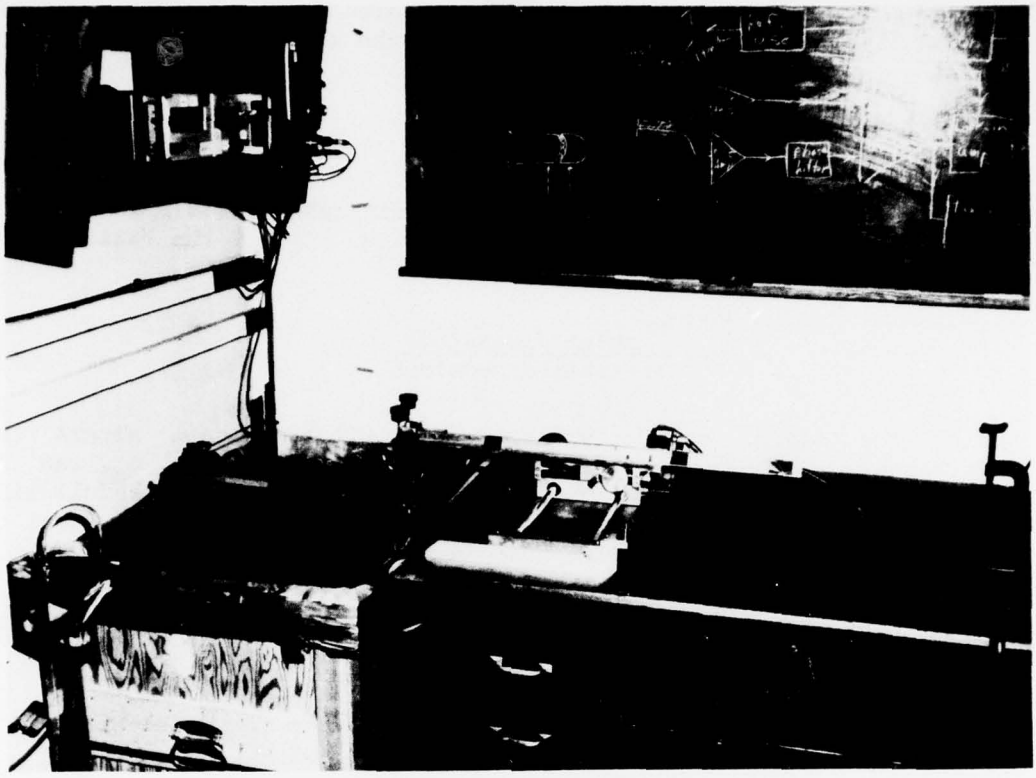

Figure 4. Electrolytic tank and x-y-z carriage assembly.

For equipotential line plots, the arm which held the probe held also a stylus on its opposite end, positioned over a sheet of drawing paper. This setup permitted a one-to-one drawing to be made of the equipotential lines around the model under test.

4. SCALING EQUATION

Electrolytic tank measurements are most useful if the model is scaled to correctly represent the charged aircraft in free space. The proper scaling factor is found by comparing the electric-field potentials calculated for the aircraft in free space and for the model in the electrolytic tank.

Consider a charged aircraft in free space. The total charge, Q_a, can be calculated from the aircraft's free-space capacitance, C_a, and the potential, V_a, of the electrostatic charge:

$$Q_a = C_a V_a \quad . \tag{1}$$

At a point distance x_a from the aircraft (center of charge), the potential, V_{xa}, can be determined from the electric-field potential equation

$$V_{xa} = \frac{kQ_a}{x_a} , \tag{2}$$

where $k = 4\pi\varepsilon_o$. (ε_o is the free-space permittivity, 8.85×10^{-12} F/m.) Scaling the aircraft reduces the capacitance, C_a, by the ratio of the scale, S, of the model, where

$$S = \frac{\text{model dimensions}}{\text{aircraft dimensions}} . \tag{3}$$

Placing the scaled model in the electrolytic tank again alters the capacitance. This new value of the model capacitance, C_m, can be calculated by first finding an equivalent sphere, R_s, for the full-size aircraft. It is calculated by setting the aircraft capacitance equal to the capacitance equation for a sphere in free space,

$$C_a = 4\pi\varepsilon_o R_s , \tag{4}$$

where R_s is given in meters. Next, R_s is scaled to the model size

$$R_m = R_s S . \tag{5}$$

Placing this scaled sphere in the electrolytic tank changes the capacitor from a single sphere type to a spherical, two-plate capacitor. The spherical capacitance, the same value as C_m, can be calculated by knowing the basket dimensions. The calculation of C_m is simplified if the basket is assumed spherical. (Appendix A data prove the validity of this assumption.) Therefore,

$$C_m = 4\pi\varepsilon_o \frac{R_b R_m}{R_b - R_m} , \tag{6}$$

where C_m is in farads, R_b is the "spherical" basket radius in meters, and R_m is the scaled sphere radius in meters.

The electrolytic tank charge, Q_m, can then be calculated by knowing the applied voltage, V_m, from the equation

$$Q_m = C_m V_m . \tag{7}$$

An equation equivalent to equation (2) for the electrolytic tank electric-field potential is

$$V_{x_m} = \frac{kQ_m}{x_m} . \tag{8}$$

Taking the ratio between equations (8) and (2) and simplifying,

$$V_{x_m} = V_{x_a}\left(\frac{Q_m}{Q_a}\right)\left(\frac{x_a}{x_m}\right), \tag{9}$$

where x_a/x_m is equivalent to 1/S. The resultant equation is

$$V_{x_m} = V_{x_a}\left(\frac{Q_m}{Q_a}\right)\left(\frac{1}{S}\right). \tag{10}$$

Thus, the electric-field potential of any point in the electrolytic tank can be compared to an equivalent point in the vicinity of a charged aircraft in free space.

5. VERIFICATION TESTS

Several tests were performed to verify the performance of both the electrolytic tank and the measurement apparatus. By using the equipotential setup, a sphere was submerged one half of its diameter into the electrolyte. The sphere configuration should produce circular equipotential lines for any given probe depth. These equipotential plots were performed for several probe depths at distances up to several sphere diameters away from the center of the sphere. These plots show that the nonspherical basket first perceptibly distorts the equipotential contours at a distance halfway between the model and the basket. The tank equipotential contours were found to be located at the

theoretically expected distances. Appendix A gives the equipotential plots obtained for the sphere in the electrolytic tank and theoretical contours computed by using the smallest basket-to-model dimension.

6. AIRCRAFT POTENTIAL DIFFERENCE AND EQUIPOTENTIAL CONTOURS

The electrolytic-tank measurements are converted to free-space measurements by use of equation (10). The charge on the F4-J aircraft was assumed to be equal to that of an equivalent-size aircraft, the F-100. This assumption was necessary due to the unavailability of either an F-100 model or an F4-J electrostatic charge information.

The Roth report[5] tabulates considerable data on the charge levels on both C-130 and F-100 aircraft. For the F-100, the charge distribution was negative 86.2 percent of the time and had a median value of -25 μC. The capacity of the aircraft was 600 pF, resulting in a median voltage of -41,700 V. The minimum charge occurring about 2.7 percent of the time was 2.5 μC resulting in a minimum of 4170 V. Charges were 2.5 μC or greater 97.3 percent of the time. This report and the data within assume the average charge of 25 μC.

An arbitrary, but known, potential difference was applied between the basket and the model aircraft in the electrolytic tank. The capacitance of the full-scale aircraft in free space is known to be approximately 600 pF. With the model scale being 1/48, the electrolytic-tank charge can be computed. By using the above information and equation (10), the full-scale potential and potential-difference contours can be obtained from the electrolytic-tank measurements.

Appendices B and C data have been converted to full-scale values for the assumed median charge of 25 μC. The minimum values can easily be determined by taking 1/10 of all labeled values since the potential and potential difference scale directly with charge. The data presented in appendix C do not include the relative-motion angle required to describe a moving target. The data correspond to a fixed target and moving projectile.

The dual-probe assembly used in taking appendix C data had long probes as opposed to minute points. The simulated probe diameter was 20 mm, and the simulated probe lengths were for a 60-mm projectile length.

7. CONCLUSIONS

Free-space electrostatic potential contours can be measured by using an electrolytic tank and a scaled-model aircraft. Accurate results are possible, provided that measurements are confined to a volume around the model less than one half the distance between the model and the basket. Future electrolytic-tank measurements should include a probe yaw angle, to account for the relative velocity of the target and projectile.

ACKNOWLEDGEMENTS

The author expresses his appreciation to Emmett Williams for his assistance on this project, both assembling the tank equipment and spending many hours taking data and converting them to the form necessary for this report; and to Theodore Blomquist, who constructed the glass probes.

LITERATURE CITED

(1) R. L. Tanner and J. E. Nanevicz, Precipitation Charging and Corona-Generated Interference in Aircraft, Stanford Research Institute, Air Force Contract AF 19 (604)--3458 (April 1961).

(2) Philip Krupen, Measuring the Electric Charge on a Missile in Flight, Harry Diamond Laboratories TR-856 (1 August 1960).

(3) Autogenous Electrification of an F-80A Airplane by 14AS-100 JATO Units, U.S. Air Force Report MCREE-50-25 (2 June 1950).

(4) R. L. Tanner and J. E. Nanevicz, An Analysis of Corona-Generated Interference in Aircraft, Proceedings of IEEE (January 1964).

(5) Alvin E. Roth, Electrostatic Charge on Aircraft in Flight, Harry Diamond Laboratories TM-69-33 (October 1969).

(6) C. E. Cooper, Corona-Generated Noise in Aircraft, Wireless World (November 1966), 547.

(7) Preliminary Investigation of Electrostatic Charging on Jet Aircraft, U.S. Air Force Report MCREE-48-52 (23 September 1948).

(8) Electrostatic Phenomena and Their Effect on Aircraft and Missiles in Flight, U.S. Air Force Report ATI No. 21578 (May 1948).

(9) Philip Krupen and Elmer B. Rogers, Measurement of Electrostatic Charge on Aircraft, Harry Diamond Laboratories TR-1267 (30 December 1964).

(10) Study and Investigation of Methods of Dissipation of Static Electricity on Helicopters, Cornell Aeronautical Laboratory, Inc., U.S. Army Contract DA44-177-TC-544 Report (September 1960).

(11) J. E. Nanevicz and R. L. Tanner, Some Techniques for Elimination of Corona Discharge Noise in Aircraft Antennas, Proceedings of IEEE (January 1964).

(12) Peter B. Johnson, Fuzing for Antiaircraft Gun Projectiles (U), Harry Diamond Laboratories TR-1553 (September 1971). (SECRET)

(13) Maxime G. Kaufman and Joseph P. Daugherty, Miss-Distance by Electrostatic Detection of Aircraft, Naval Research Laboratory Report 4593 (1 December 1955).

(14) Philip Krupen, An Electrostatic Proximity Fuze for a 40-mm Shell, Harry Diamond Laboratories TR-493 (1 August 1957).

(15) Philip Krupen, The Feasibility of a Passive Electrostatic Fuze for Antimissile Missiles, Harry Diamond Laboratories TR-579 (28 February 1959).

(16) P. Krupen, An Electrostatic Fuzing System for Antimissile Missiles, Harry Diamond Laboratories TR-1025 (26 March 1962).

(17) Philip Krupen, A DC Capacitance Fuze, Harry Diamond Laboratories TR-1095 (15 February 1963).

(18) Edward A. White, Jr., James E. Swanekamp, and Gerald P. Worrell, DC Capacitive Fuzing System for Small Projectiles, Naval Ordnance Laboratory NOLTR 65-59 (18 May 1965).

(19) C. L. Fortescue and S. W. Farnsworth, Trans. AIEE, 32 (1913), 893.

(20) H. Barkhausen and J. Bruck, Elektrotech. Z., 54 (1933), 175.

(21) John A. Simpson, Jr., A Scanning Device for Plotting Equipotential Lines, The Review of Scientific Instruments, 12 (January 1941), 37.

(22) Paul E. Green, Jr., Automatic Plotting of Electrostatic Fields, The Review of Scientific Instruments, 19, No. 10 (October 1948).

(23) R. W. Atkinson, Trans. AIEE, 38 (1919), 983.

APPENDIX A.--EQUIPOTENTIAL PLOTS AROUND THE TEST SPHERE

FIGURES

APPENDIX A

The adequacy of the electrolytic tank simulation was verified as follows: A test sphere 8.8 cm in diameter was submerged in the tank's electrolyte to a depth equal to its radius, and a voltage (2 V) was applied between the sphere and the basket. Equipotential contours were plotted by using the apparatus described in the main body of the report. Plots were made for seven different depths. Figures A-1 to A-7 are plots of the results. The small circles are actual data points, and the solid lines represent the theoretical contours.

The potential at a point x_m in the tank is given by

$$V_{x_m} = Q_m\left(\frac{1}{x_m} - \frac{1}{R_b}\right) = V_m\left(\frac{\frac{R_b}{x_m} - 1}{\frac{R_b}{R_m} - 1}\right)$$

relative to the screen, where

V_{x_m} = potential of a point located x_m from the basket, in meters,

CURVE	ELECTROLYTIC-TANK POTENTIAL (V)	FREE-SPACE POTENTIAL (V)
A	0.5	0.85
B	0.75	1.10
C	1.0	1.35
D	1.5	1.85
E	2.0	2.35

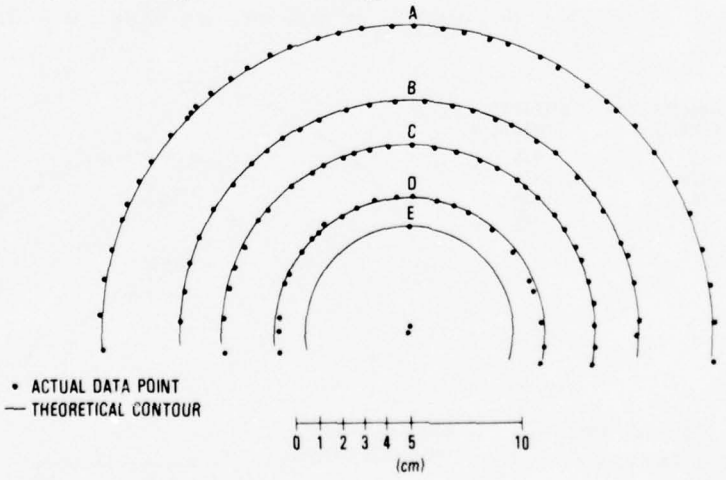

Figure A-1. Equipotential plots around test sphere; probe depth = 0 cm.

APPENDIX A

Q_m = charge on the model, in coulombs,

x_m = point between the basket and the test sphere (referenced to the basket location),

R_b = basket radius in meters,

V_m = potential applied to the test sphere, in volts (referenced to the basket),

R_m = test sphere radius, in meters.

If the dimensions of the tank are allowed to approach infinity while Q_m is held constant, then the potential is simply

$$V_{x_m} = \frac{Q_m}{x_m} .$$

For the equivalent free-space condition (infinite tank), then the potential at all points is larger than that measured by a constant amount,

$$\Delta V = \frac{V_m}{\frac{R_b}{R_m} - 1} .$$

Here, V_m = 2 V, R_b = 29.5 cm, and R_m = 4.4 cm, so that ΔV = 0.35 V.

CURVE	ELECTROLYTIC-TANK POTENTIAL (V)	FREE-SPACE POTENTIAL (V)
A	0.5	0.85
B	0.75	1.10
C	1.0	1.35
D	1.5	1.85
E	2.0	2.35

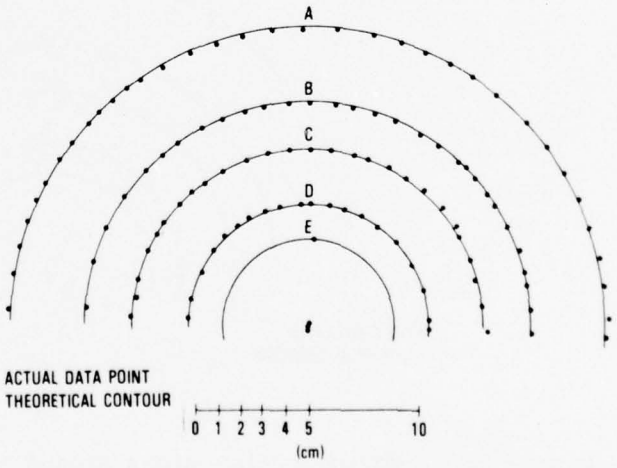

Figure A-2. Equipotential plots around test sphere; probe depth = 2 cm.

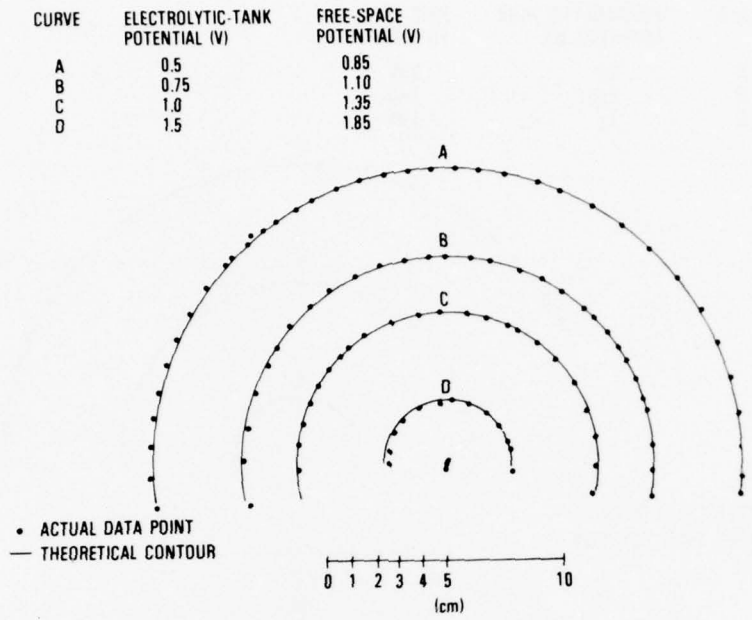

Figure A-3. Equipotential plots around test sphere; probe depth = 5 cm.

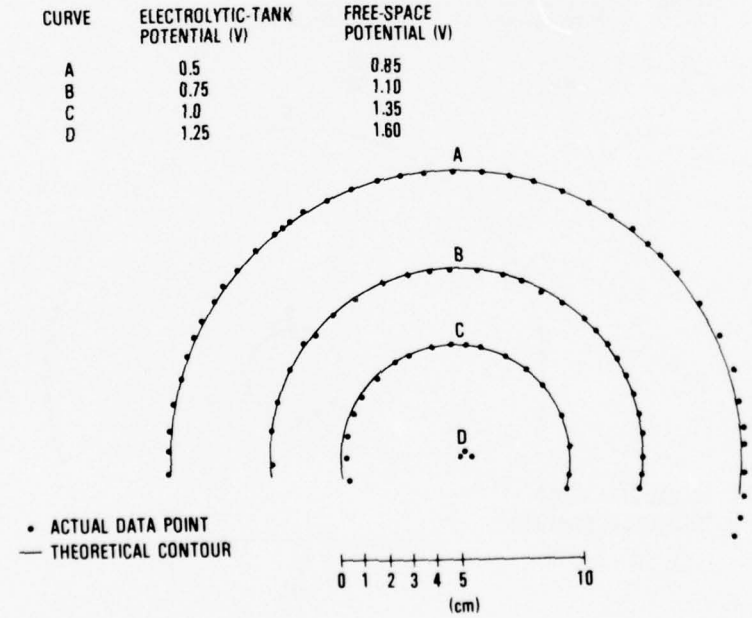

Figure A-4. Equipotential plots around test sphere; probe depth = 6.2 cm.

APPENDIX A

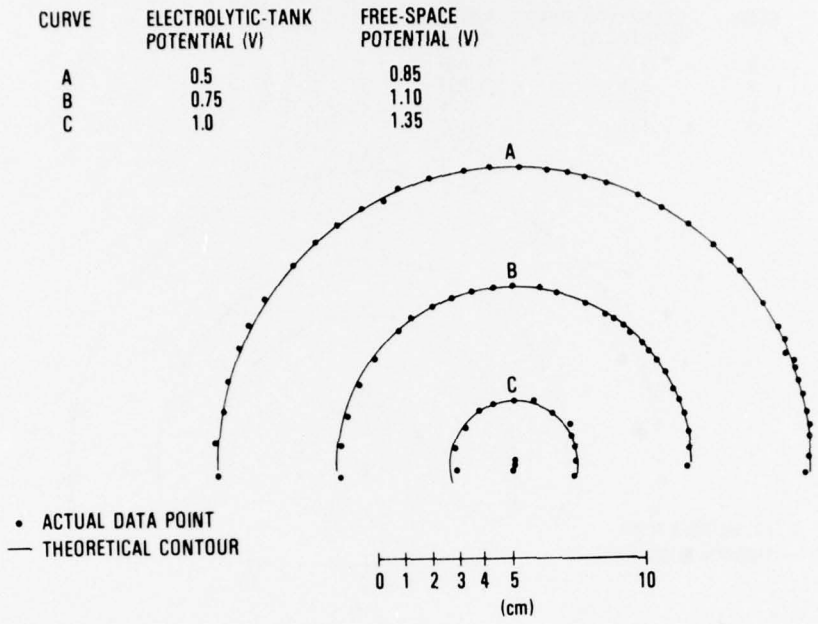

Figure A-5. Equipotential plots around test sphere; probe depth = 7.3 cm.

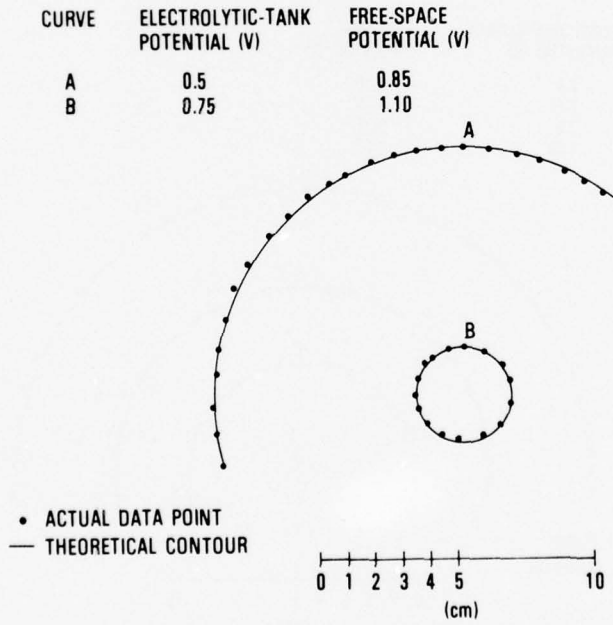

Figure A-6. Equipotential plots around test sphere; probe depth = 9.7 cm.

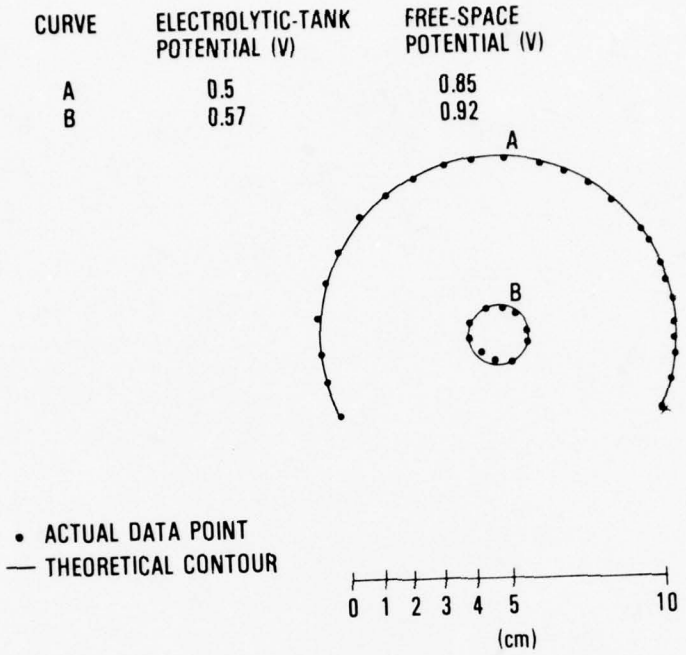

Figure A-7. Equipotential plots around test sphere; probe depth = 11.9 cm.

APPENDIX B.--EQUIPOTENTIAL LINE CONTOUR PLOTS AROUND AN AIRCRAFT

FIGURES

APPENDIX B

A 1/48 scale model of an F4-J aircraft was metalized by using silver ribbon and conducting epoxy paint. The model was submerged into the electrolyte a distance of one half the wing span. Figure B-1 describes the appropriate orientations. A voltage difference of 2 V was applied between the model and the basket.

Equipotential contour lines were plotted by using the test apparatus described in the main body of this report. Each contour line, as shown in figures B-2 to B-9, has been translated into the free space for a full-size aircraft, assuming an aircraft potential of 41,700 V and a capacitance value of 600 pF.

The circles on each equipotential contour plot are data points that have been transformed from the value measured in the electrolytic tank to the value measured in free space. A best-fit curve for the data points is represented by the solid line.

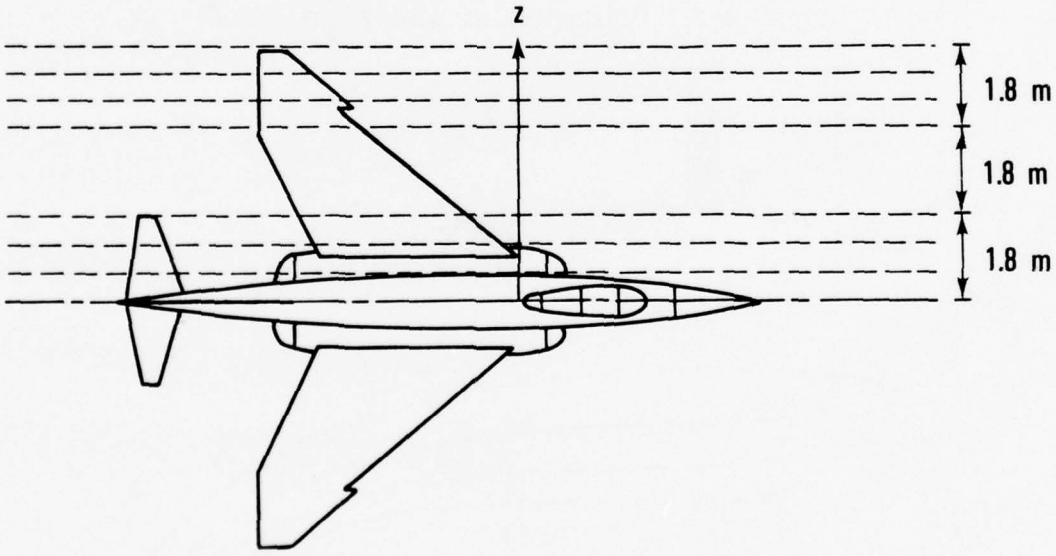

Figure B-1. Equipotential probe orientations with respect to aircraft.

APPENDIX B

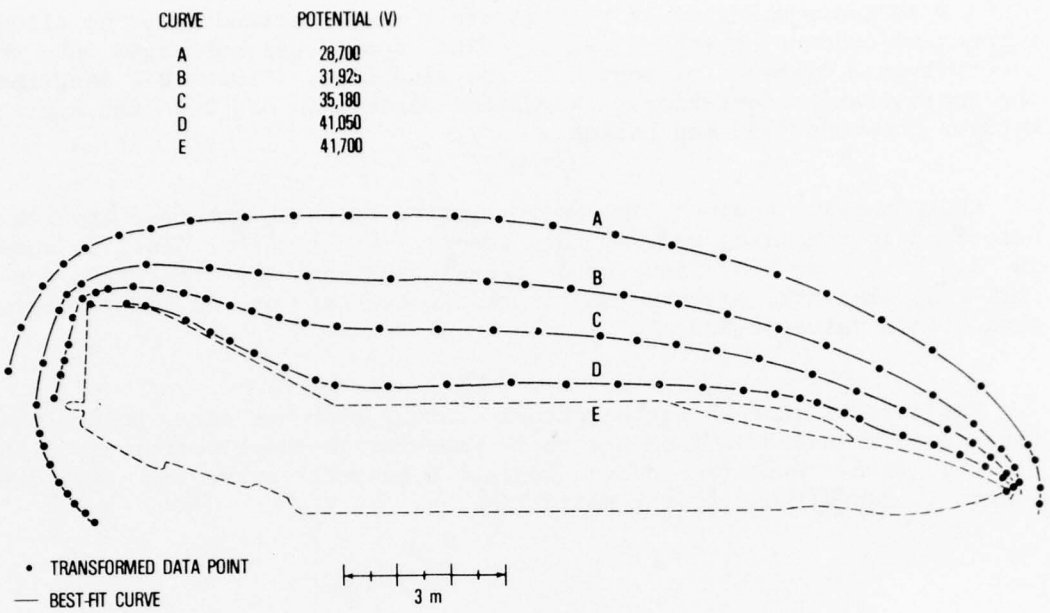

Figure B-2. Equipotential plot for z = 0 m.

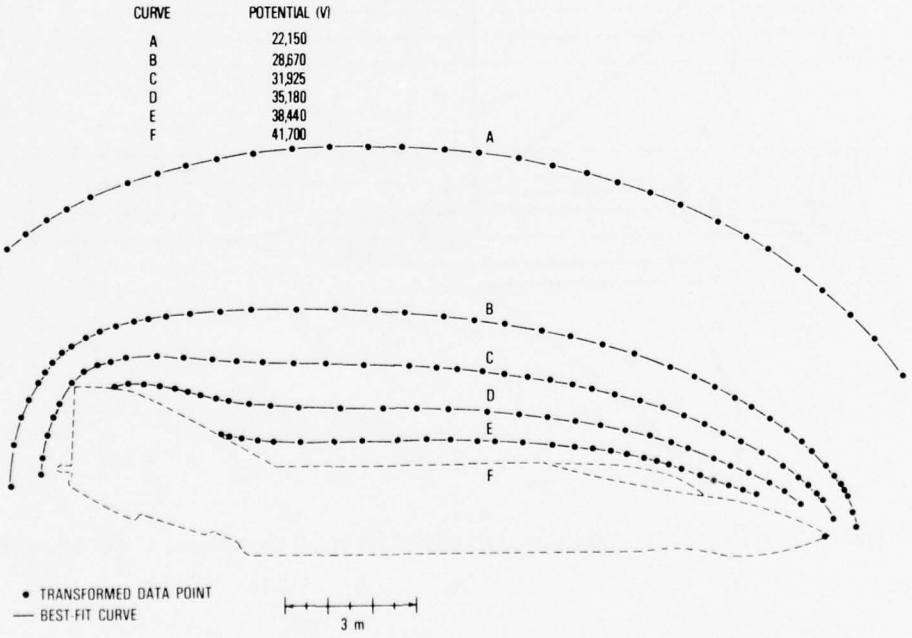

Figure B-3. Equipotential plot for z = 0.6 m.

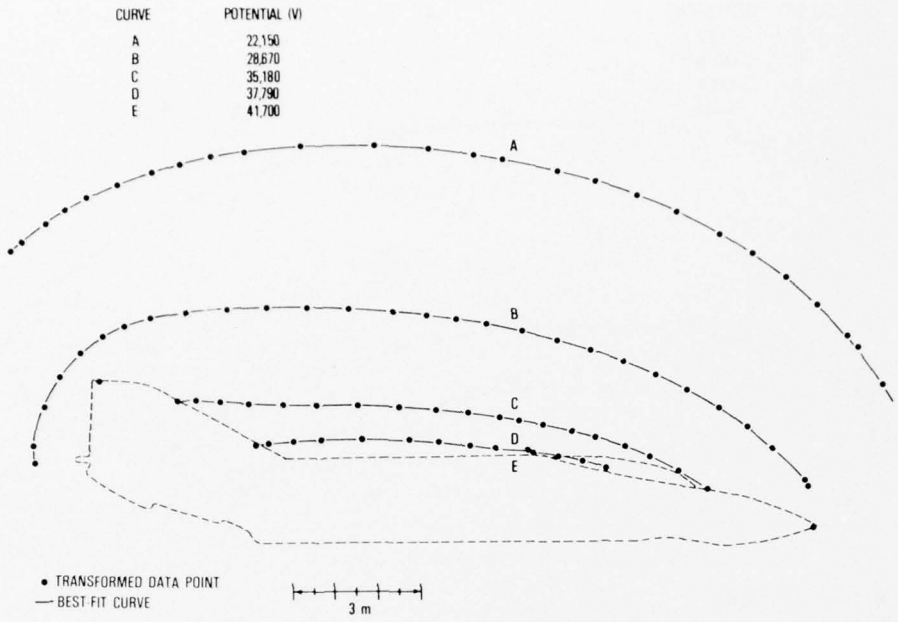

Figure B-4. Equipotential plot for z = 1.2 m.

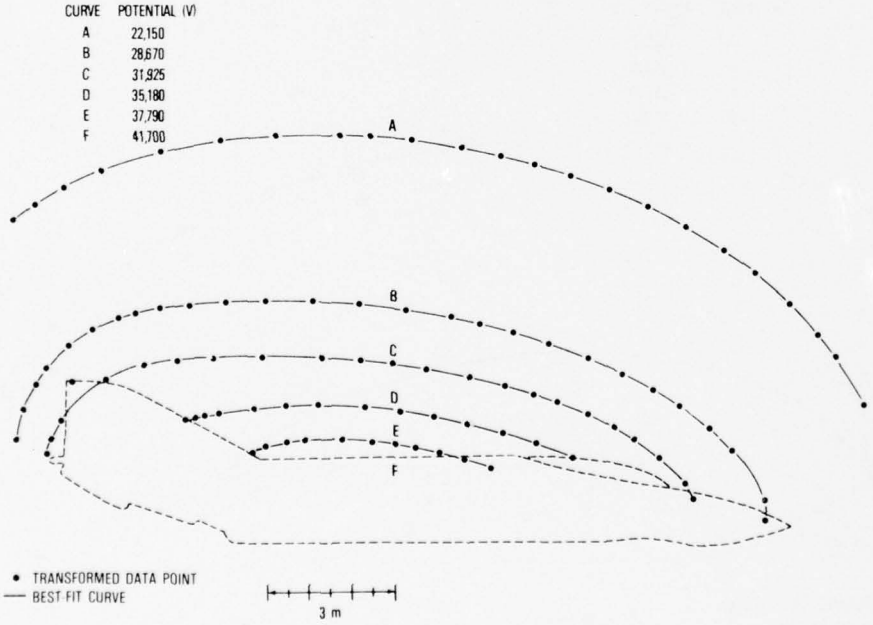

Figure B-5. Equipotential plot for z = 1.8 m.

APPENDIX B

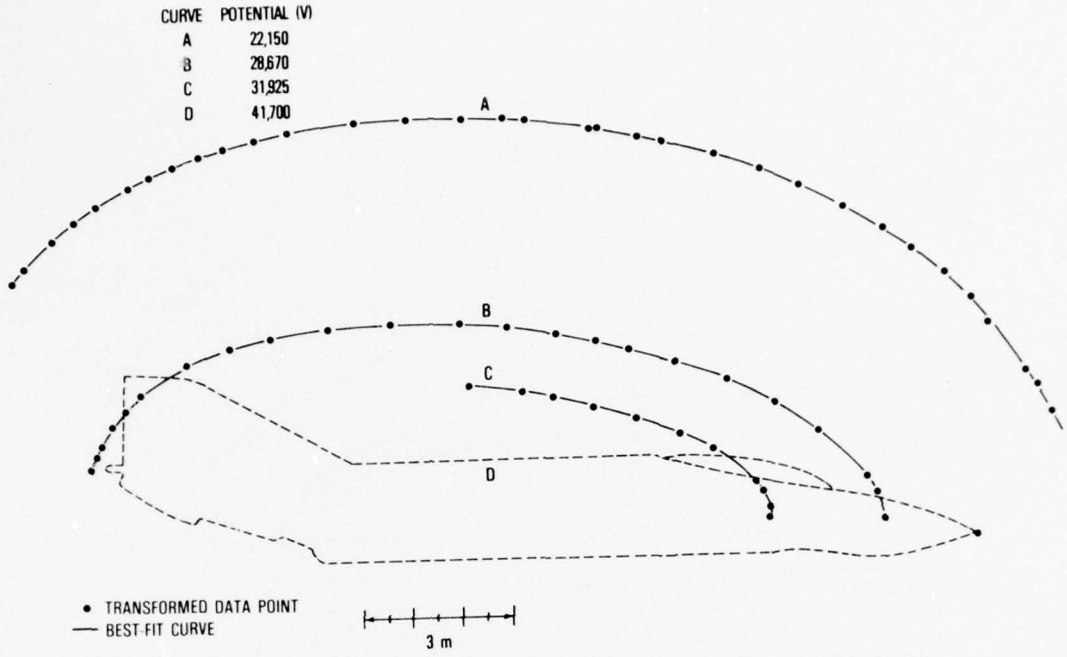

Figure B-6. Equipotential plot for z = 3.6 m.

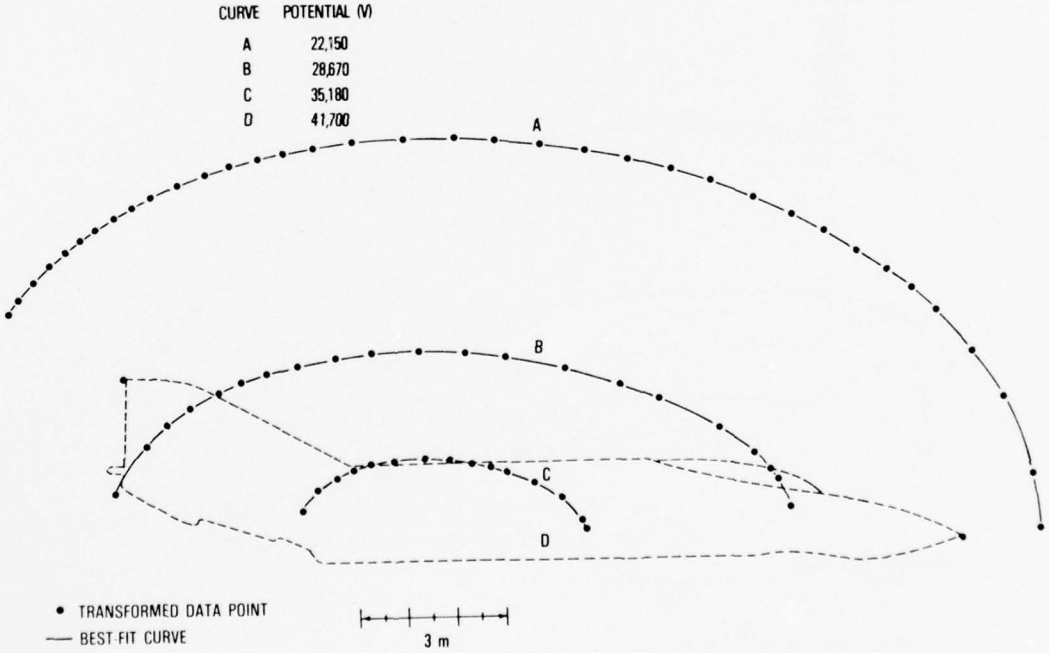

Figure B-7. Equipotential plot for z = 4.2 m.

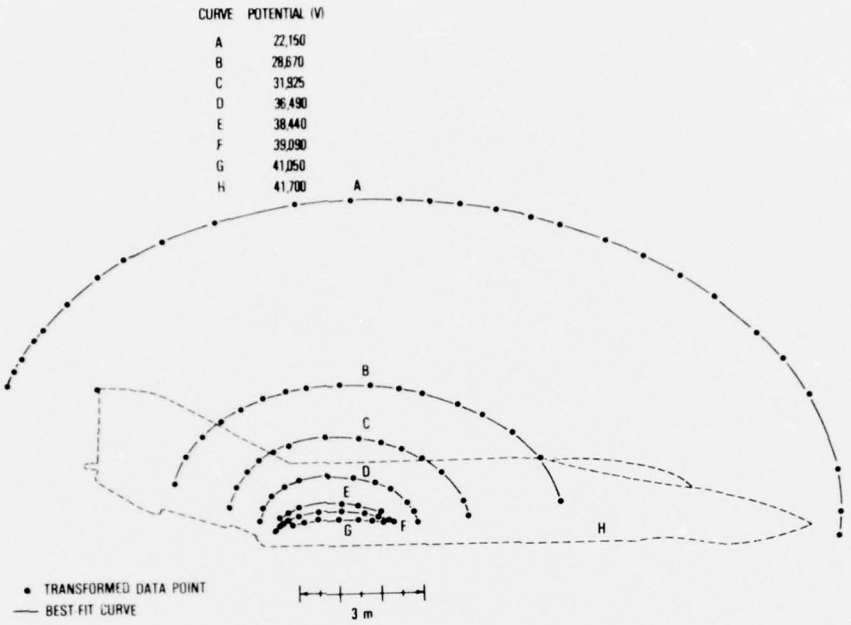

Figure B-8. Equipotential plot for z = 4.8 m.

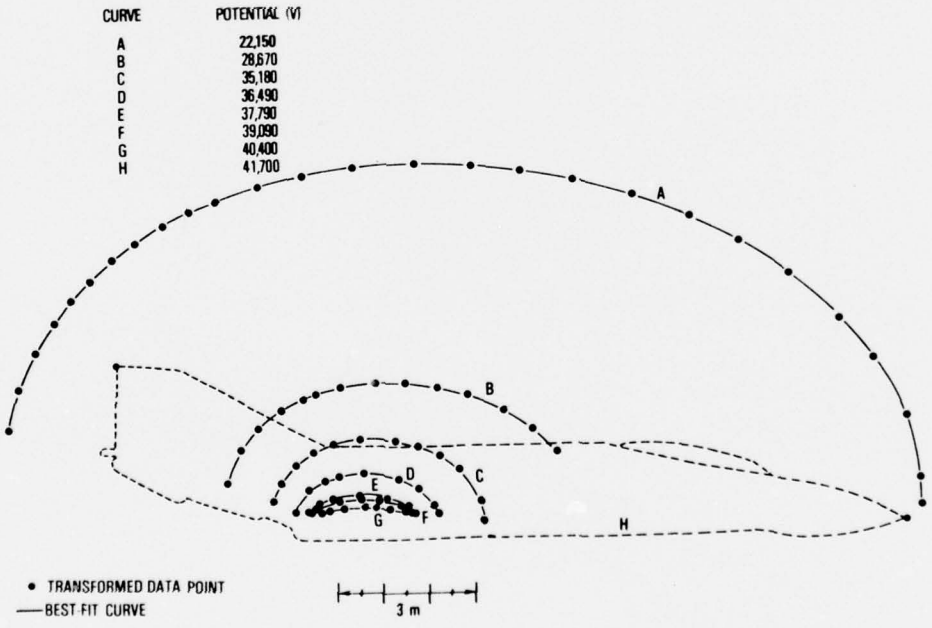

Figure B-9. Equipotential plot for z = 5.4 m.

APPENDIX C.--DUAL-PROBE POTENTIAL-DIFFERENCE PLOTS FOR AIRCRAFT FLYBYS

FIGURES

APPENDIX C

FIGURES (Cont'd)

A 1/48 scale model of an F4-J aircraft was metalized by using silver ribbon and conducting epoxy paint. The model was submerged into the electrolyte a distance of one half the wing span. A voltage difference of 1 V was applied between the model and the basket. Figure C-1 defines (arrows) the direction of the flybys. The position with respect to the reference point also is defined. The flyby voltages for various α and β angles and different y positions are plotted in figures C-2 to C-44.

The data are presented as converted values corresponding to the equivalent signal for a 60-mm round in the full scale free space, where an aircraft surface potential of 41,700 V is assumed.

A baseline (zero potential difference) is indicated for each curve. The dotted reference line locates the signature with respect to the aircraft. The physical distance corresponding to the length of the voltage curves is approximately equal to the length of the aircraft.

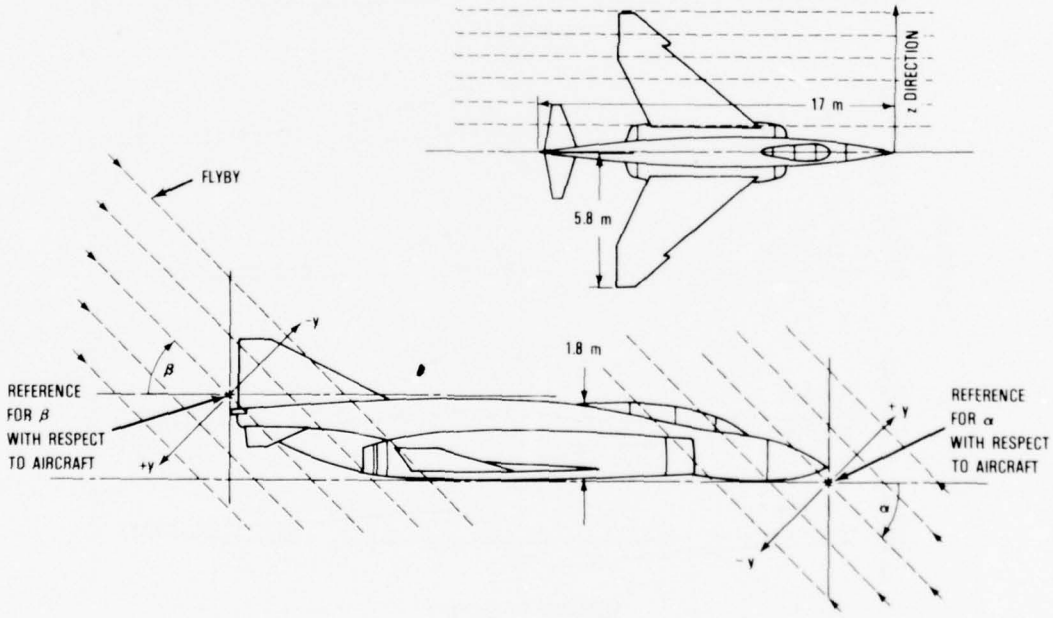

Figure C-1. Dual-probe flyby orientations in respect to aircraft.

APPENDIX C

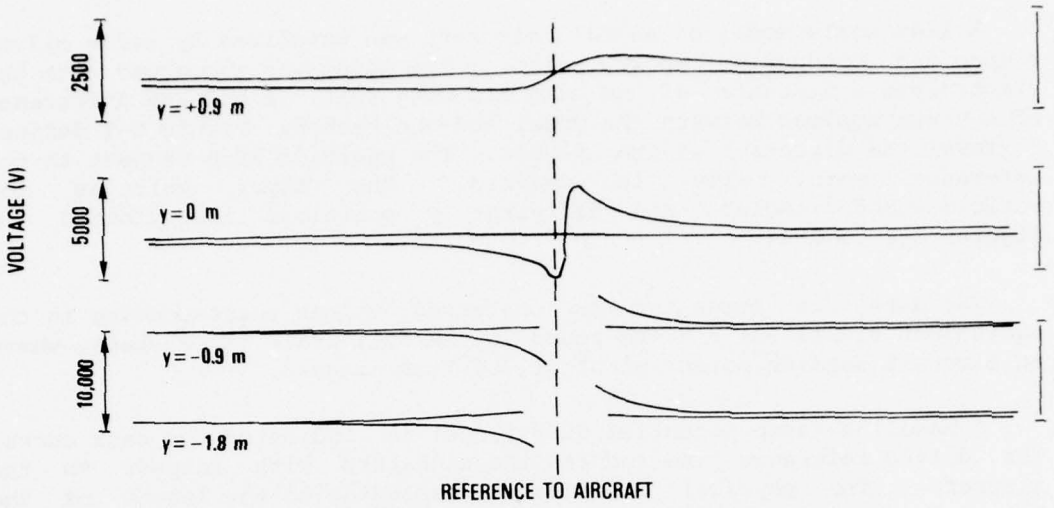

Figure C-2. Potential-difference plot for α = 90 deg, z = 0 m.

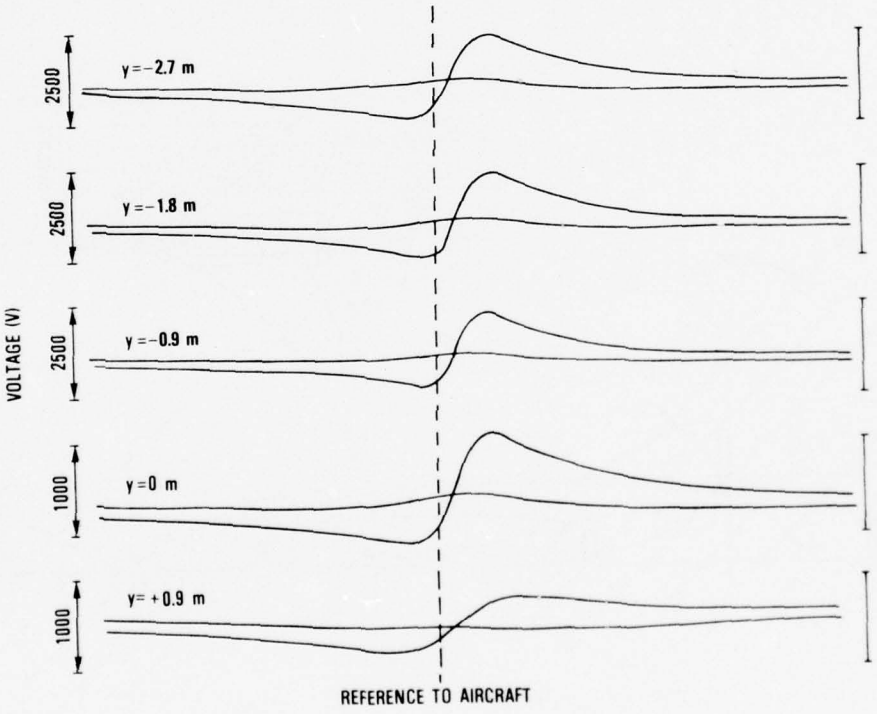

Figure C-3. Potential-difference plot for α = 90 deg, z = 0.9 m.

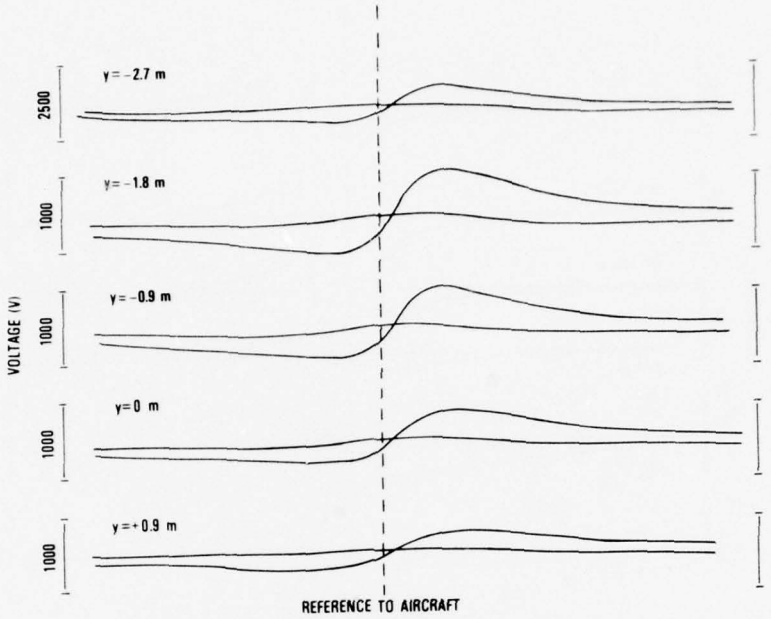

Figure C-4. Potential-difference plot for α = 90 deg, z = 1.8 m.

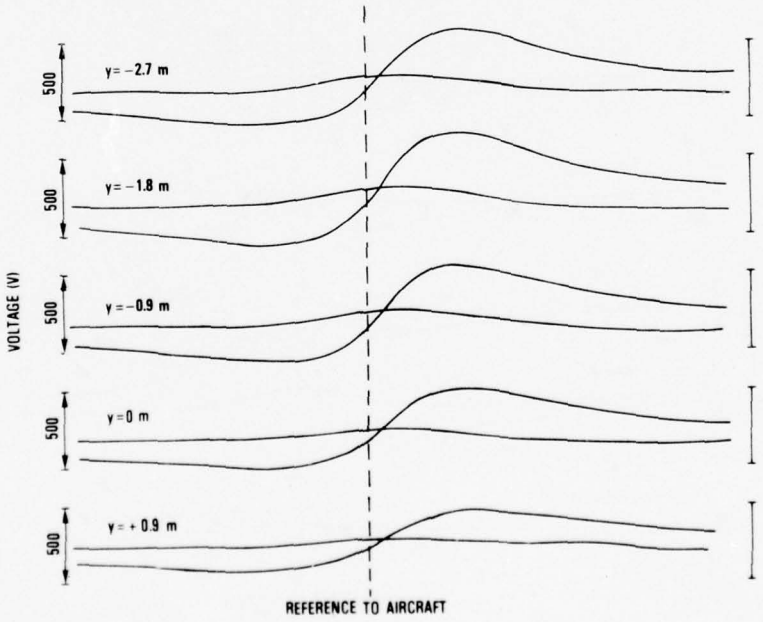

Figure C-5. Potential-difference plot for α = 90 deg, z = 2.7 m.

APPENDIX C

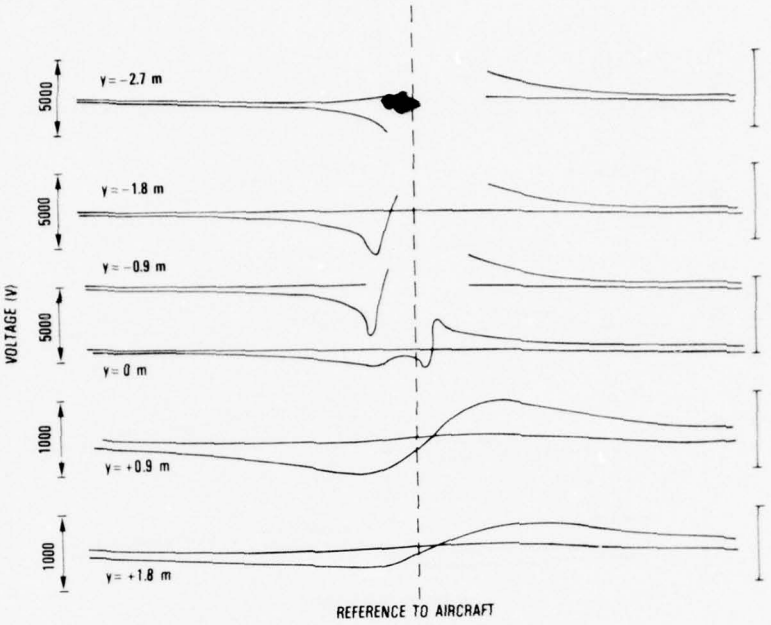

Figure C-6. Potential-difference plot for β = 90 deg, z = 0 m.

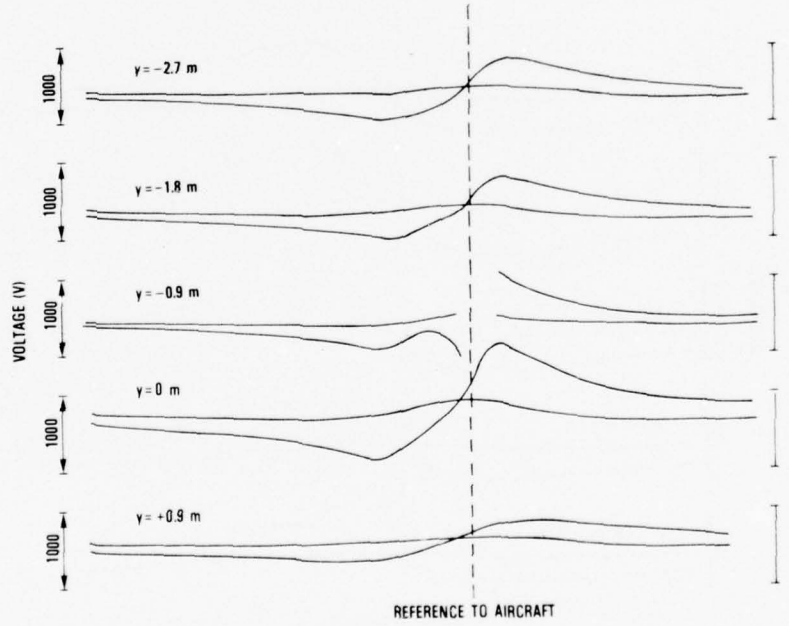

Figure C-7. Potential-difference plot for β = 90 deg, z = 0.9 m.

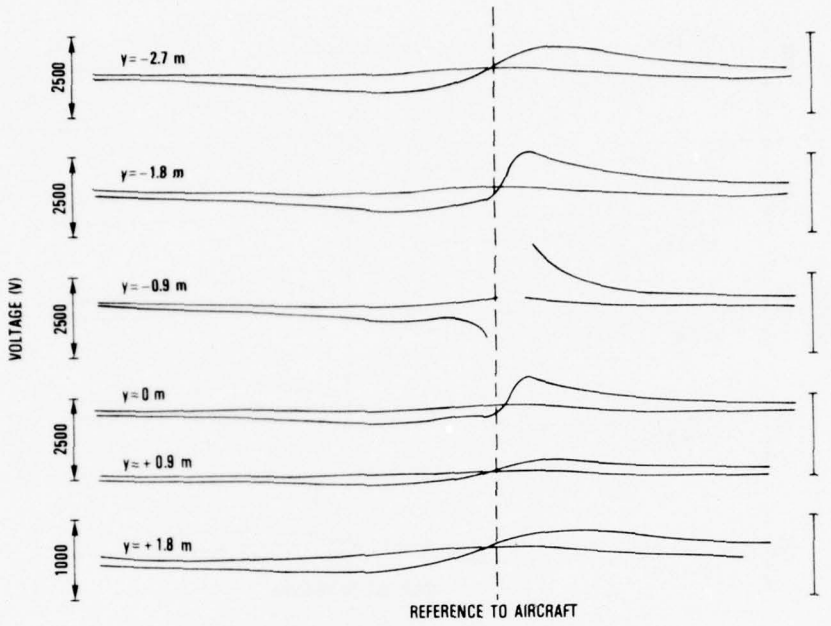

Figure C-8. Potential-difference plot for β = 90 deg, z = 1.8 m.

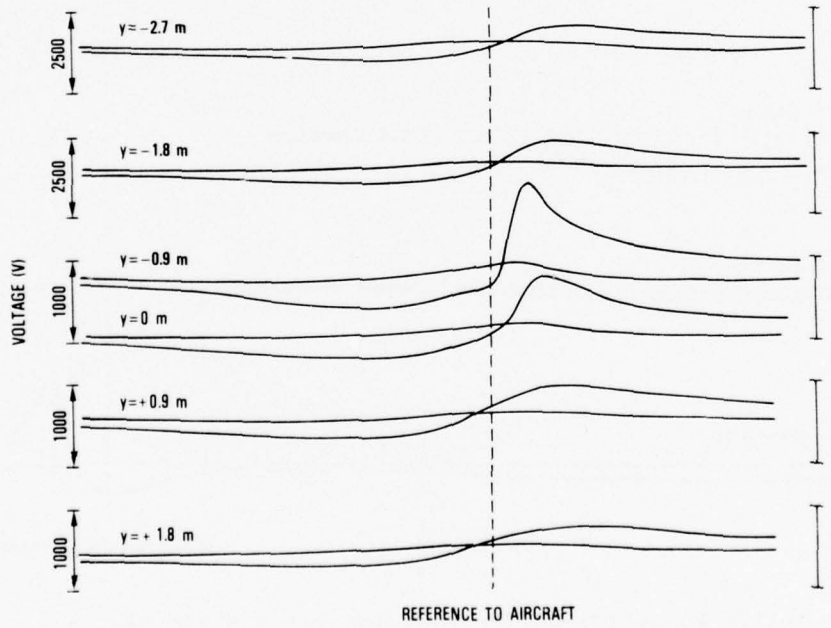

Figure C-9. Potential-difference plot for β = 90 deg, z = 2.7 m.

APPENDIX C

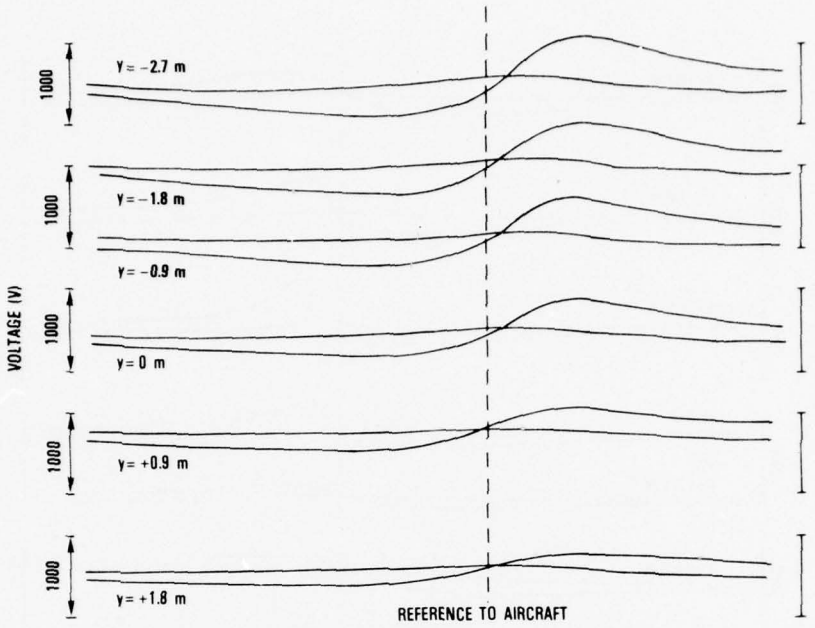

Figure C-10. Potential-difference plot for β = 90 deg, z = 3.6 m.

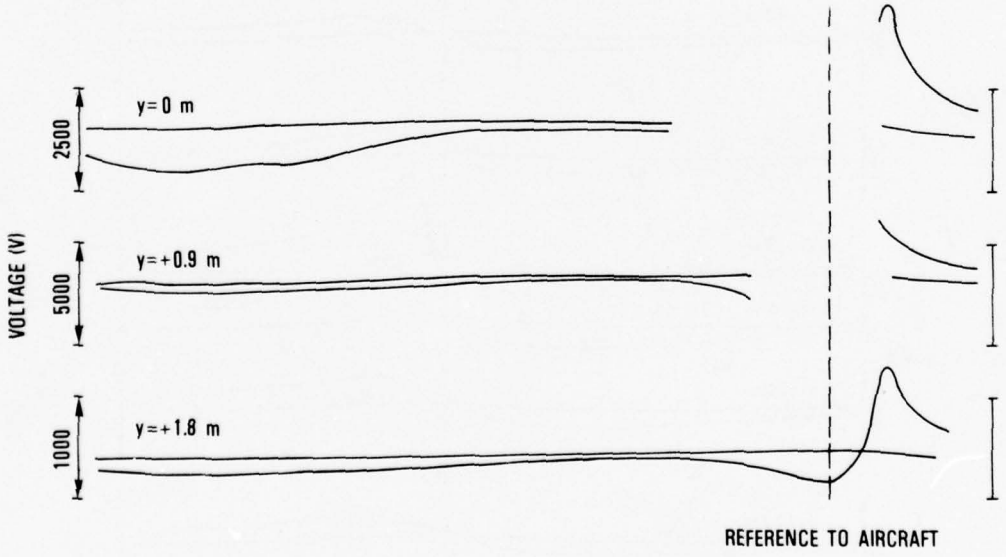

Figure C-11. Potential-difference plot for β = 180 deg, z = 0 m.

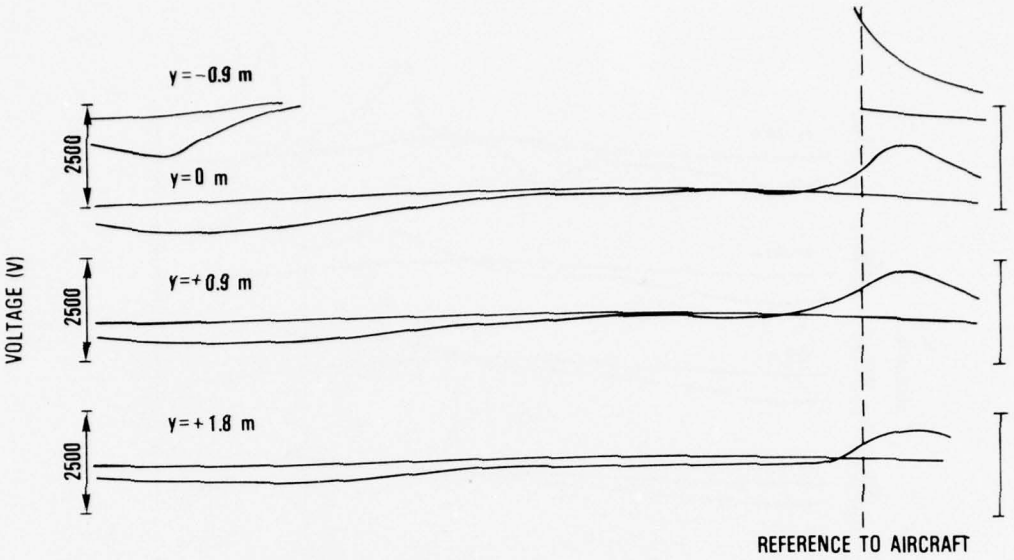

Figure C-12. Potential-difference plot for β = 180 deg, z = 0.9 m.

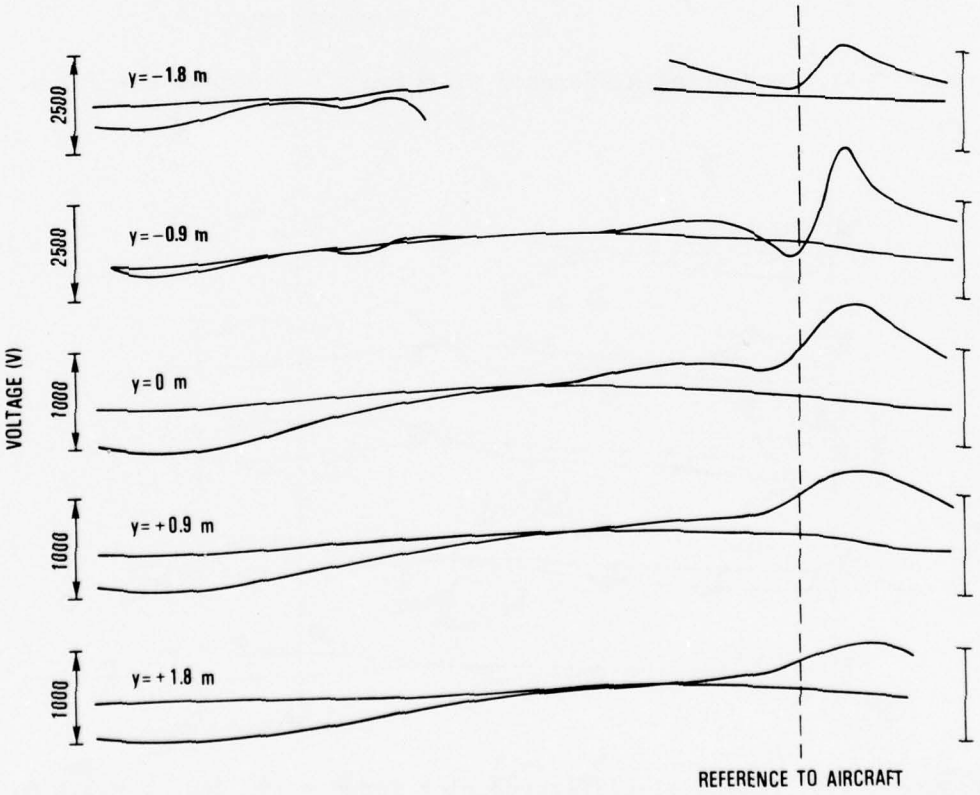

Figure C-13. Potential-difference plot for β = 180 deg, z = 1.8 m.

APPENDIX C

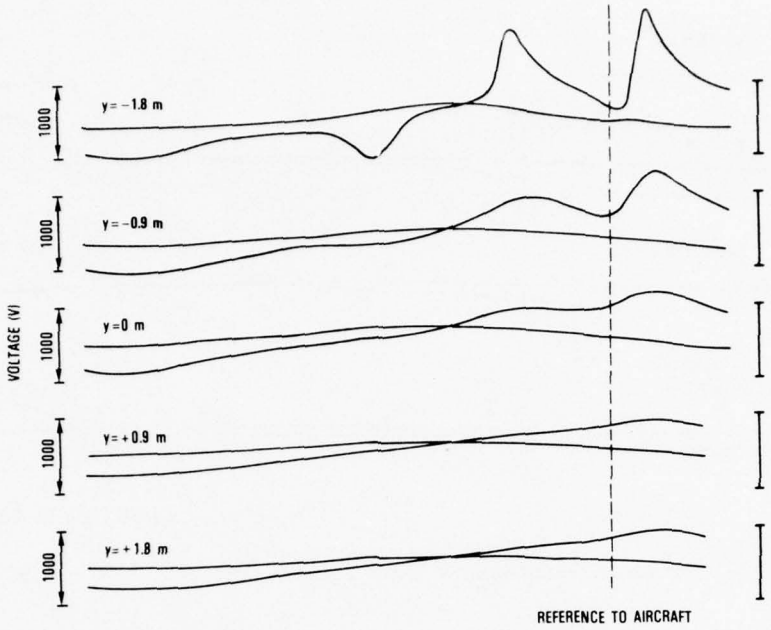

Figure C-14. Potential-difference plot for β = 180 deg, z = 2.7 m.

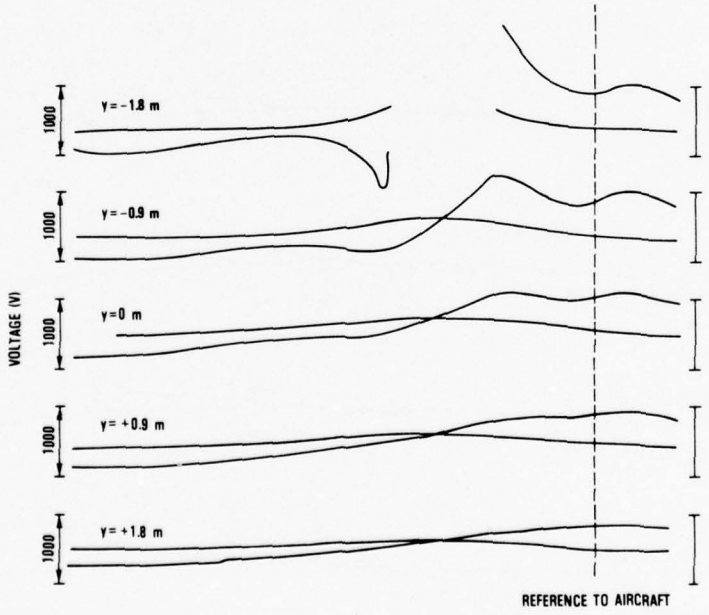

Figure C-15. Potential-difference plot for β = 180 deg, z = 3.6 m.

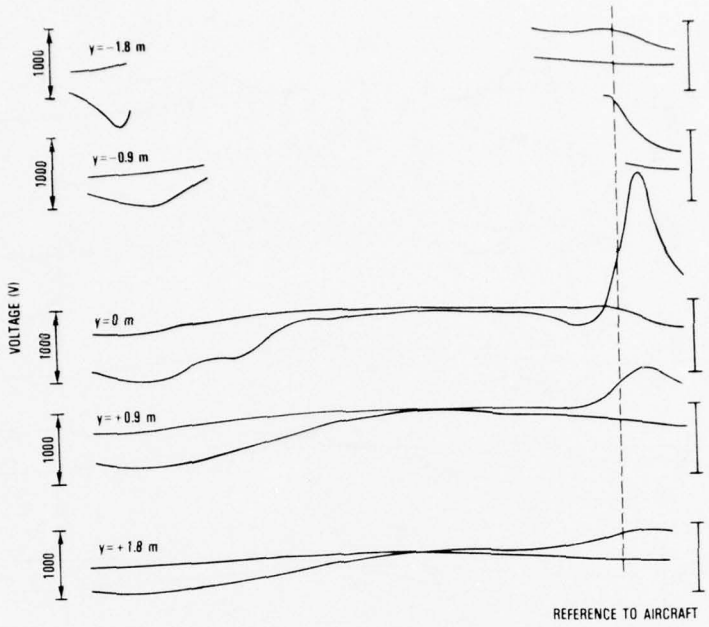

Figure C-16. Potential-difference plot for α = 180 deg, z = 0 m.

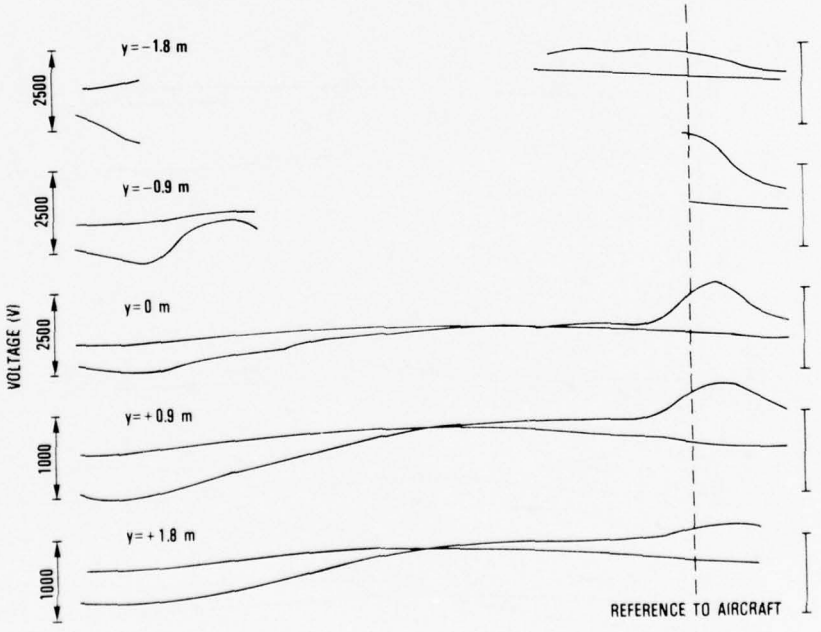

Figure C-17. Potential-difference plot for α = 180 deg, z = 0.9 m.

APPENDIX C

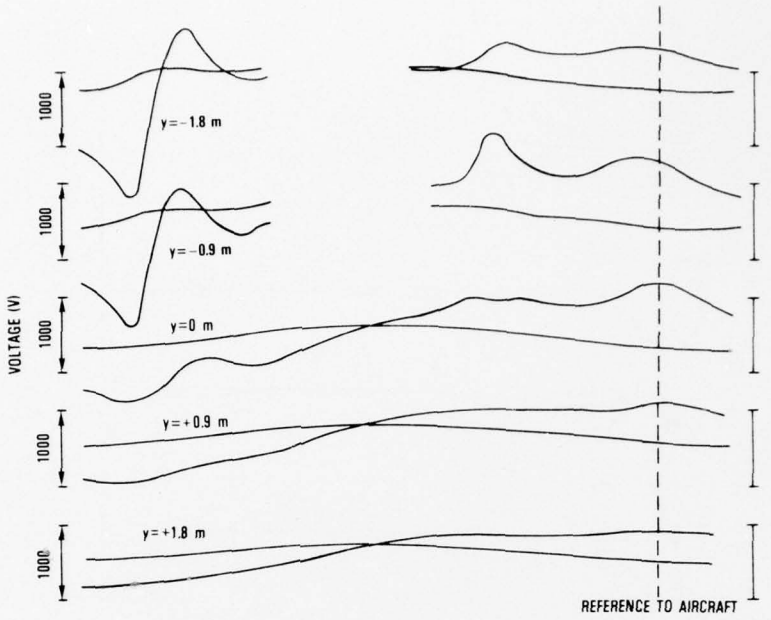

Figure C-18. Potential-difference plot for α = 180 deg, z = 1.8 m.

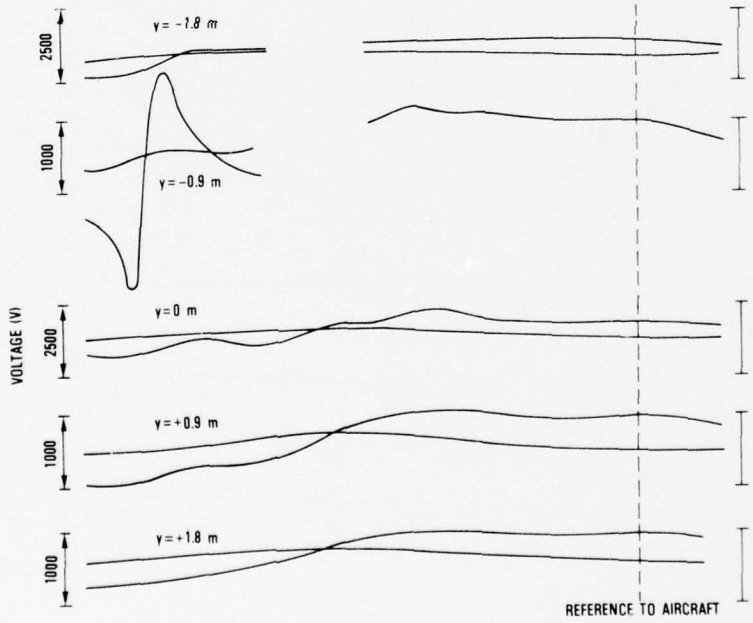

Figure C-19. Potential-difference plot for α = 180 deg, z = 2.7 m.

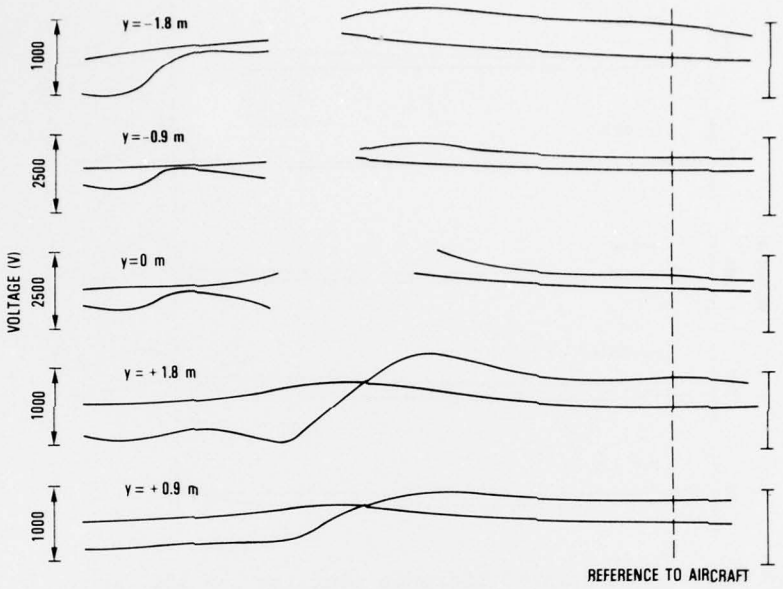

Figure C-20. Potential-difference plot for α = 180 deg, z = 3.6 m.

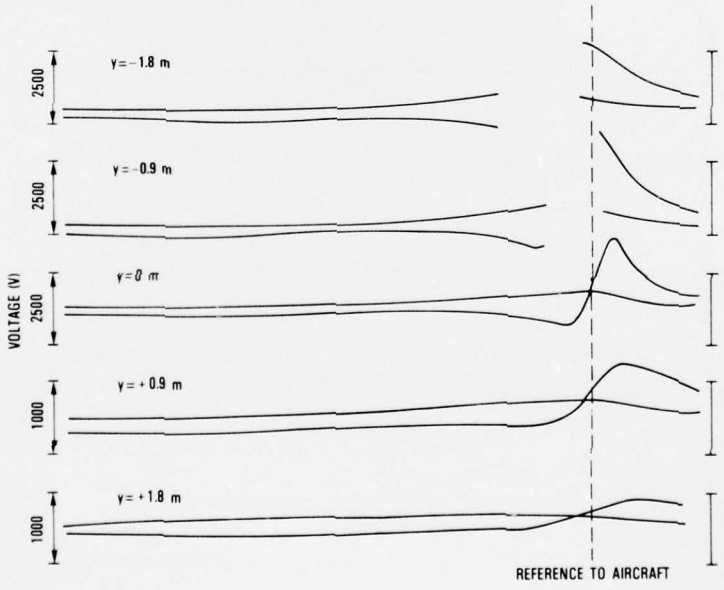

Figure C-21. Potential-difference plot for α = 150 deg, z = 0 m.

APPENDIX C

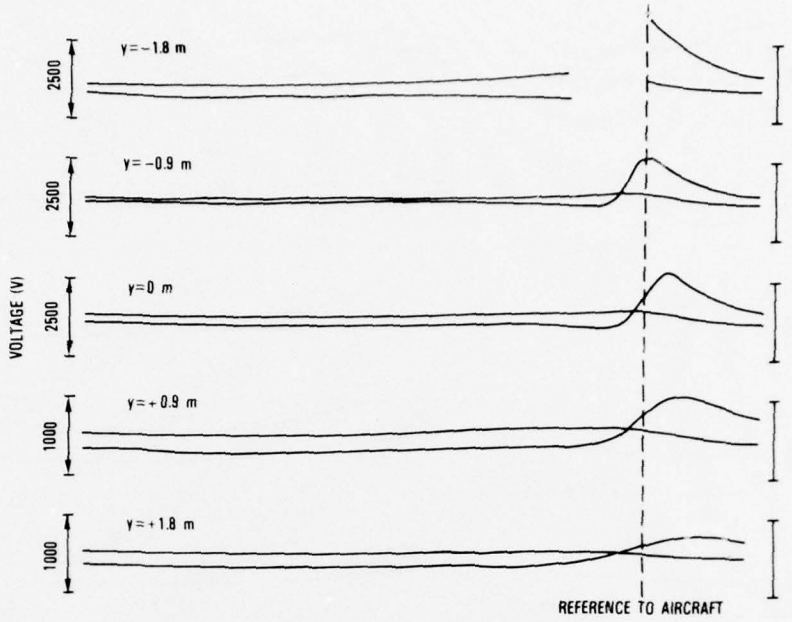

Figure C-22. Potential-difference plot for α = 150 deg, z = 0.9 m.

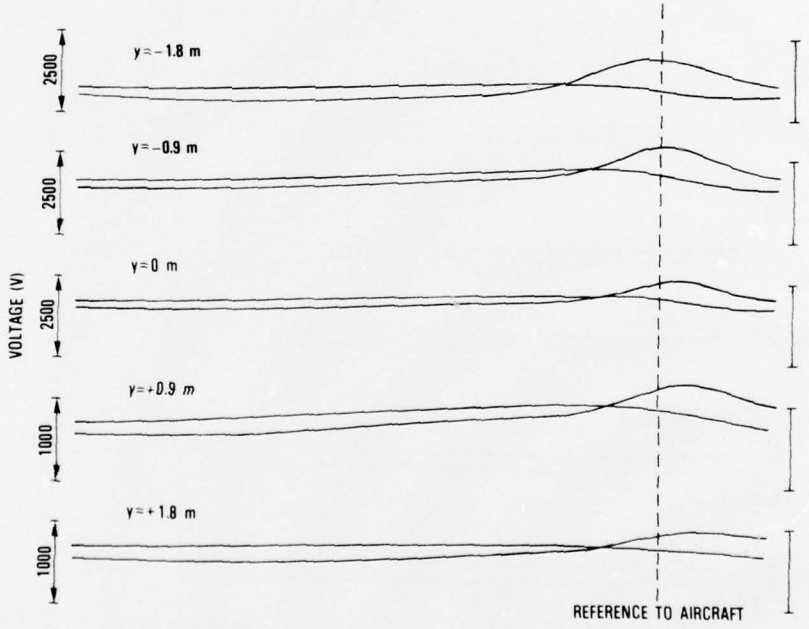

Figure C-23. Potential-difference plot for α = 150 deg, z = 1.8 m.

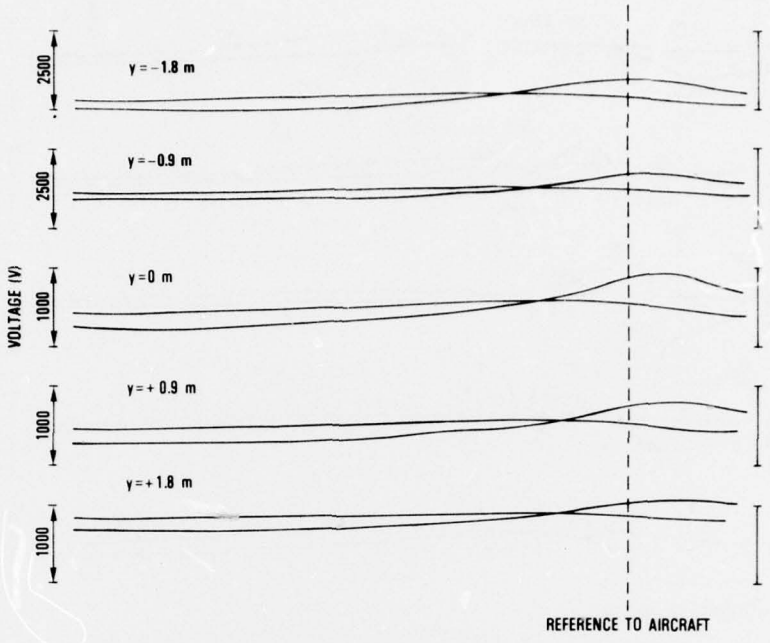

Figure C-24. Potential-difference plot for α = 150 deg, z = 2.7 m.

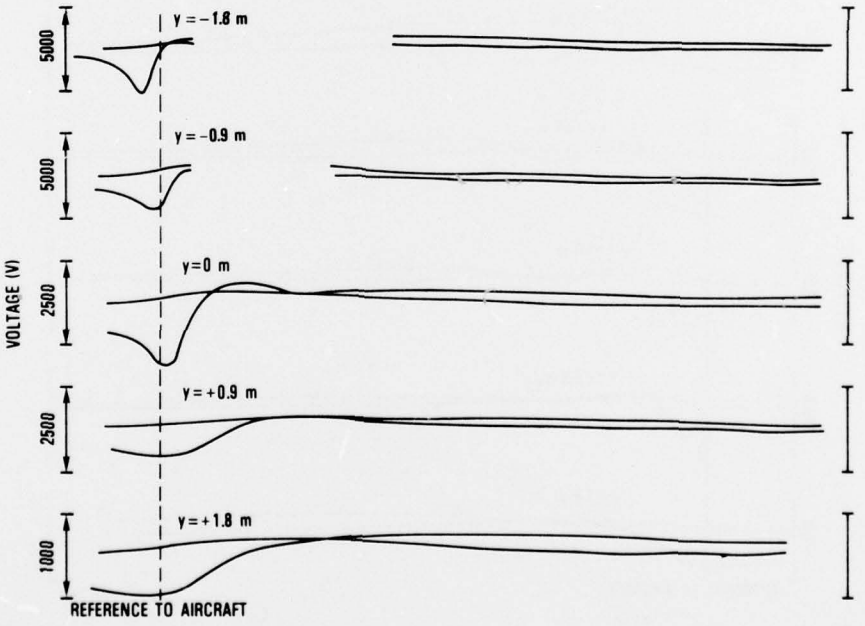

Figure C-25. Potential-difference plot for β = 60 deg, z = 0 m.

APPENDIX C

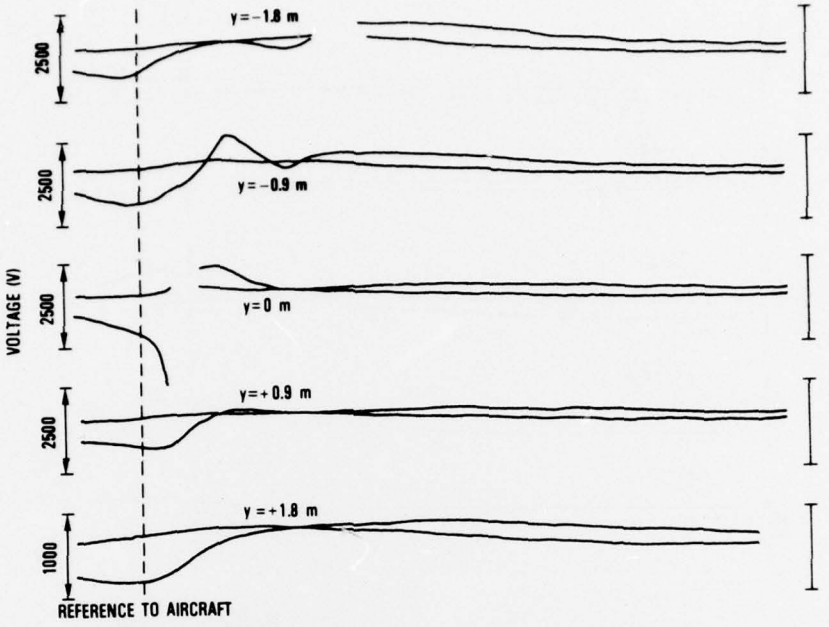

Figure C-26. Potential-difference plot for β = 60 deg, z = 0.9 m.

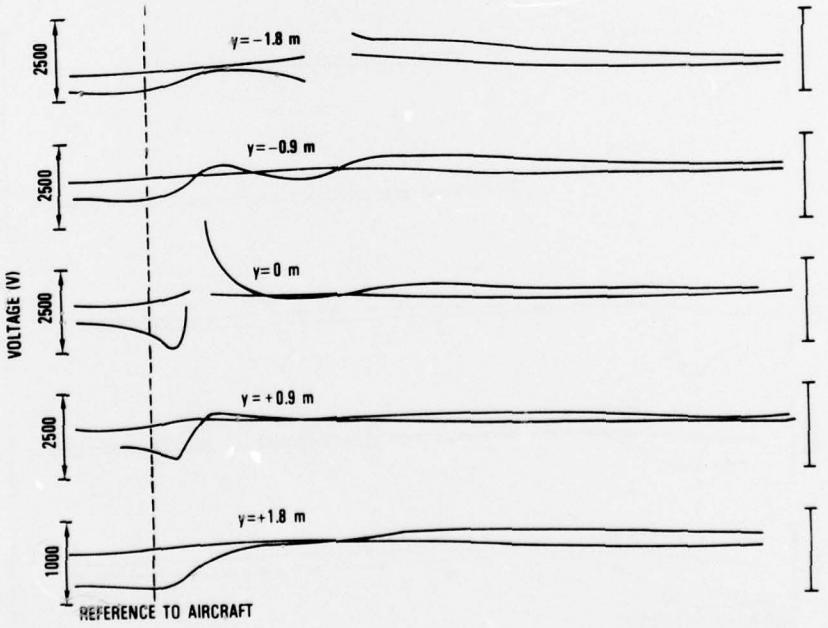

Figure C-27. Potential-difference plot for β = 60 deg, z = 1.8 m.

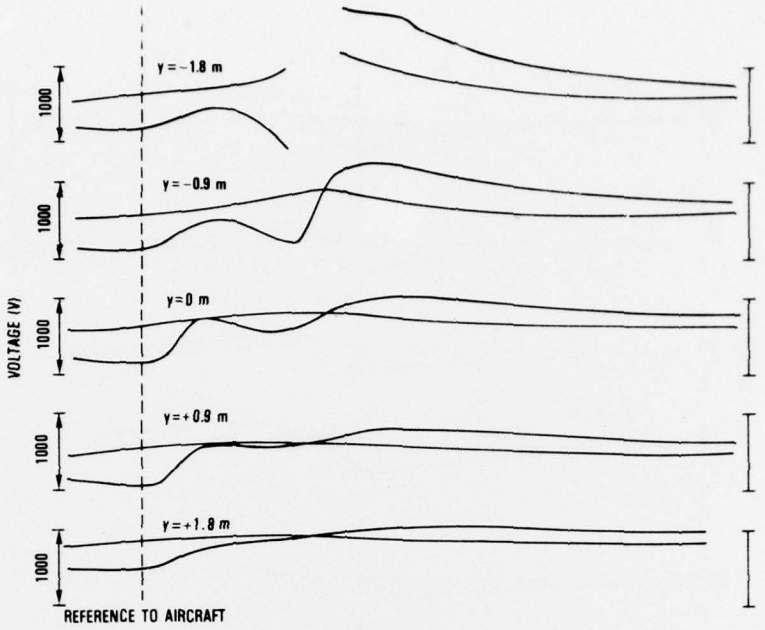

Figure C-28. Potential-difference plot for β = 60 deg, z = 2.7 m.

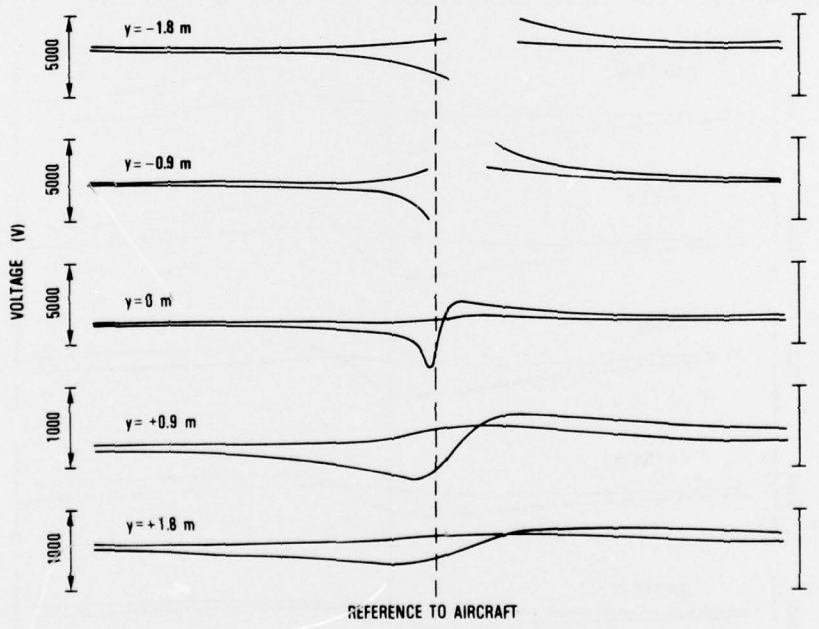

Figure C-29. Potential-difference plot for α = 30 deg, z = 0 m.

APPENDIX C

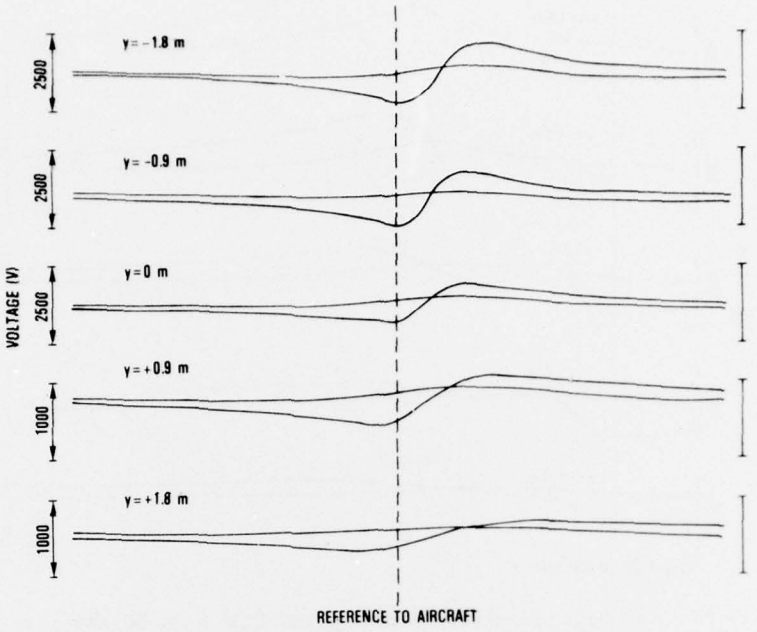

Figure C-30. Potential-difference plot for α = 30 deg, z = 0.9 m.

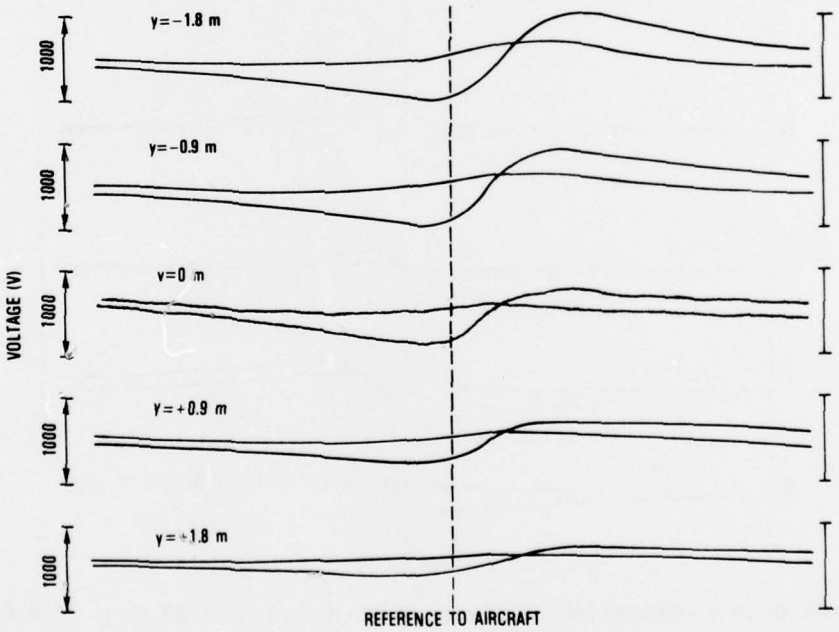

Figure C-31. Potential-difference plot for α = 30 deg, z = 1.8 m.

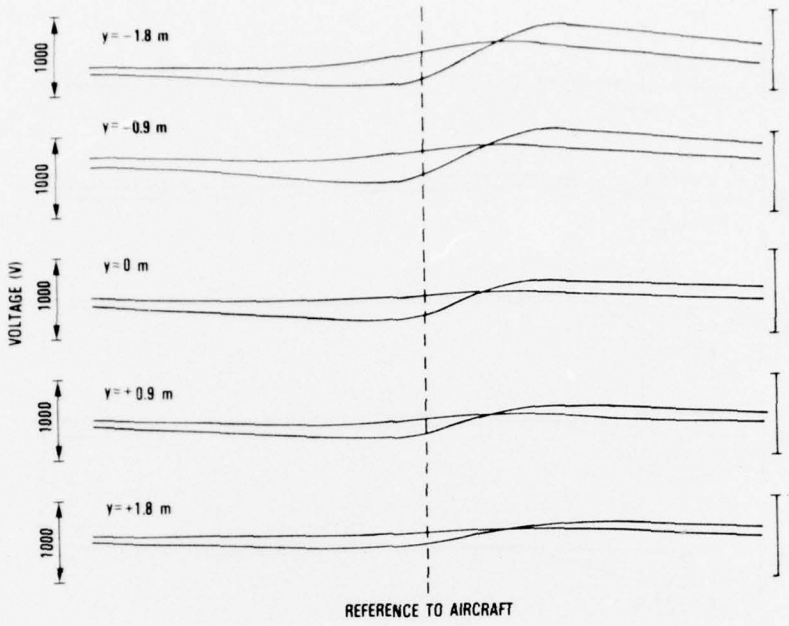

Figure C-32. Potential-difference plot for α = 30 deg, z = 2.7 m.

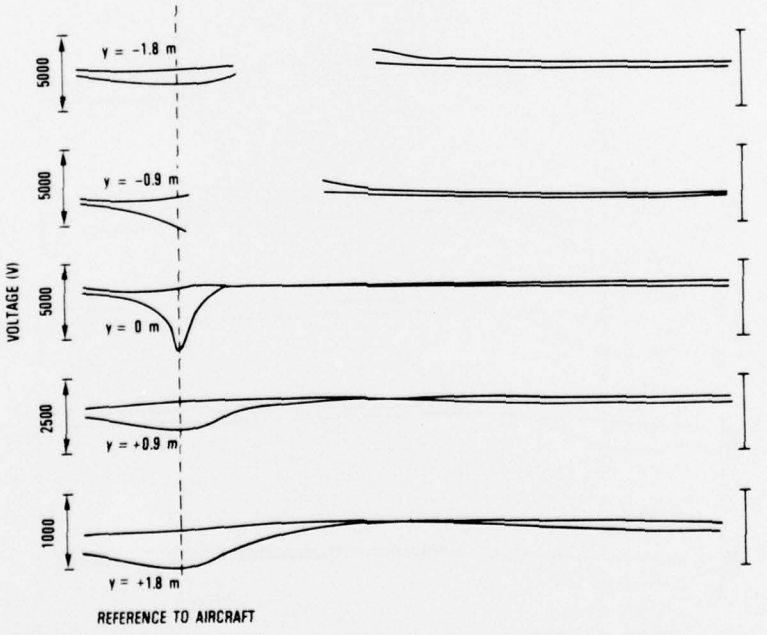

Figure C-33. Potential-difference plot for α = 60 deg, z = 0 m.

APPENDIX C

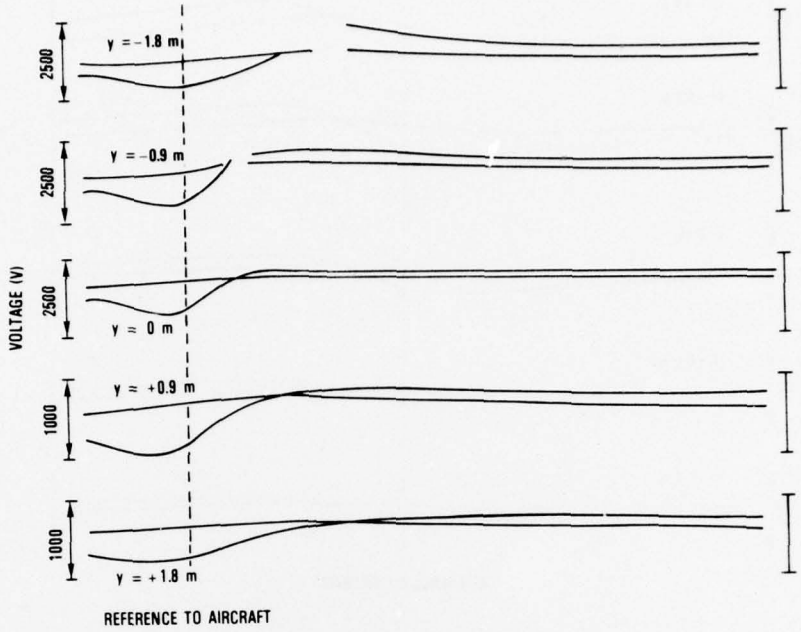

Figure C-34. Potential-difference plot for α = 60 deg, z = 0.9 m.

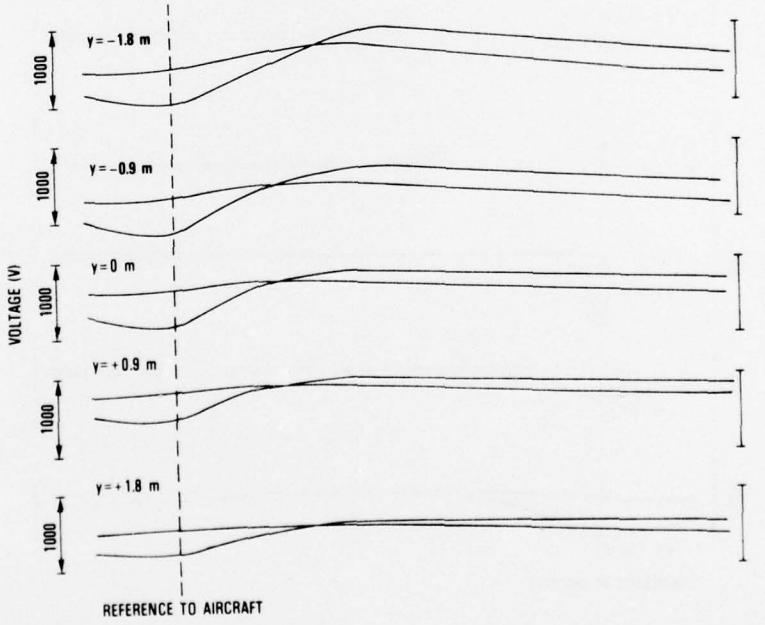

Figure C-35. Potential-difference plot for α = 60 deg, z = 1.8 m.

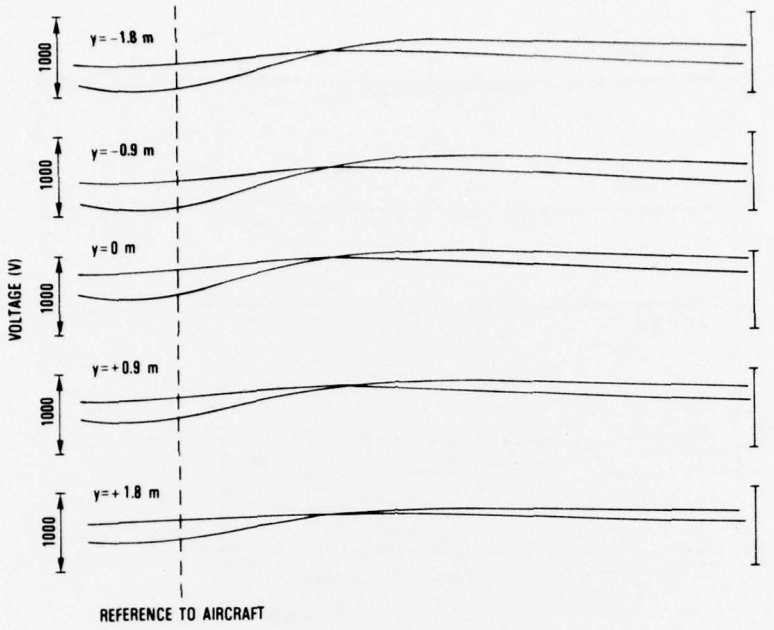

Figure C-36. Potential-difference plot for α = 60 deg, z = 2.7 m.

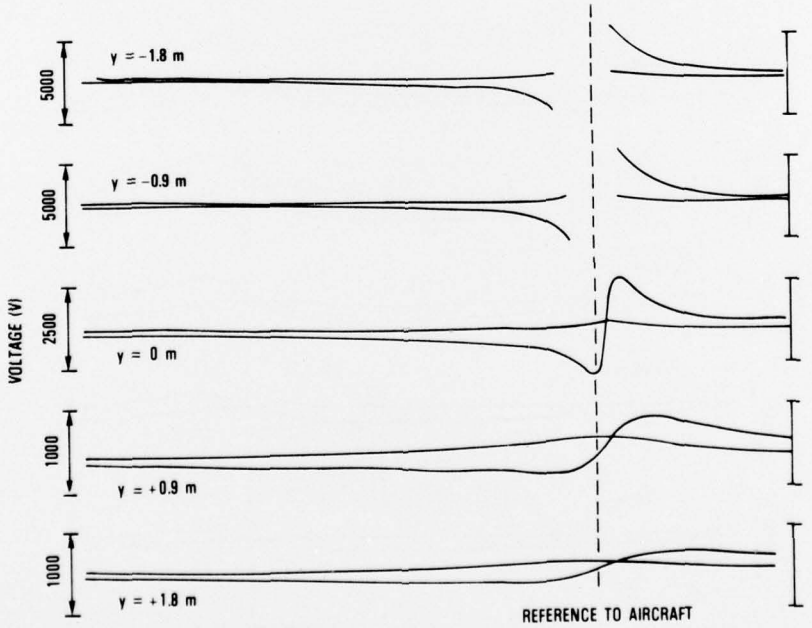

Figure C-37. Potential-difference plot for α = 120 deg, z = 0 m.

APPENDIX C

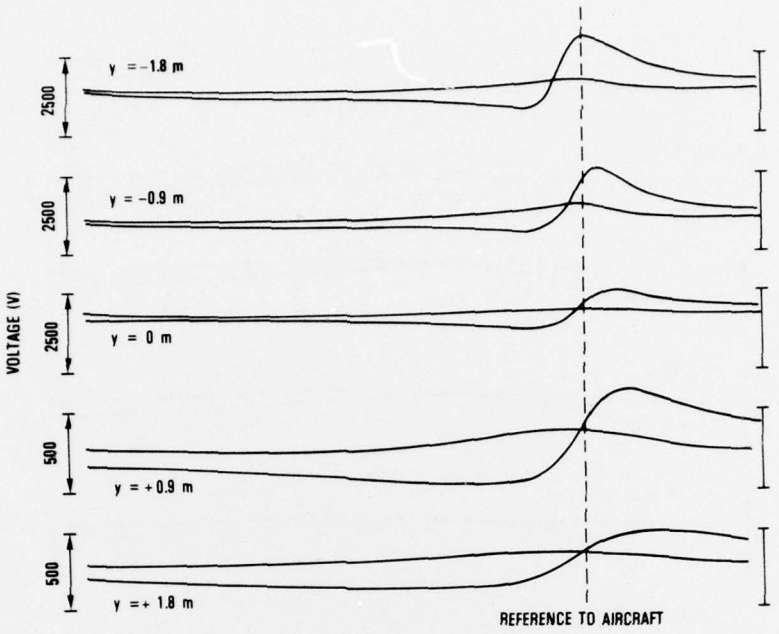

Figure C-38. Potential-difference plot for α = 120 deg, z = 0.9 m.

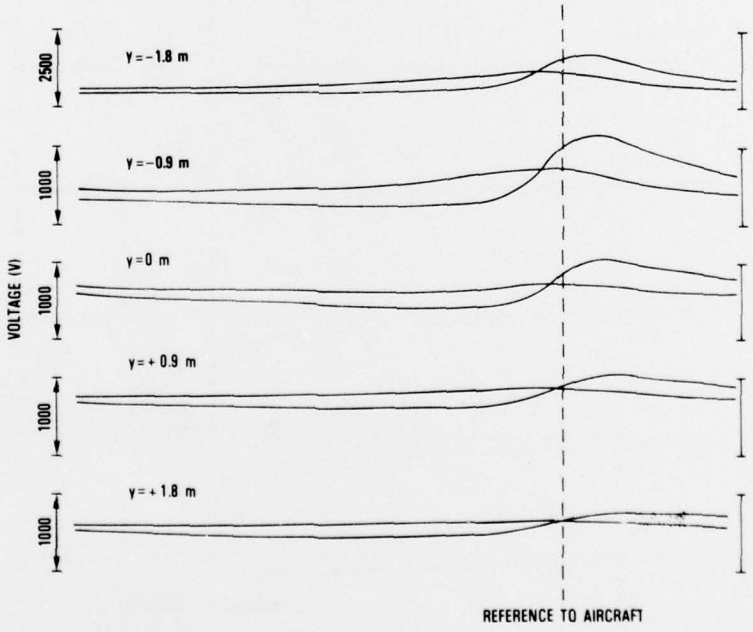

Figure C-39. Potential-difference plot for α = 120 deg, z = 1.8 m.

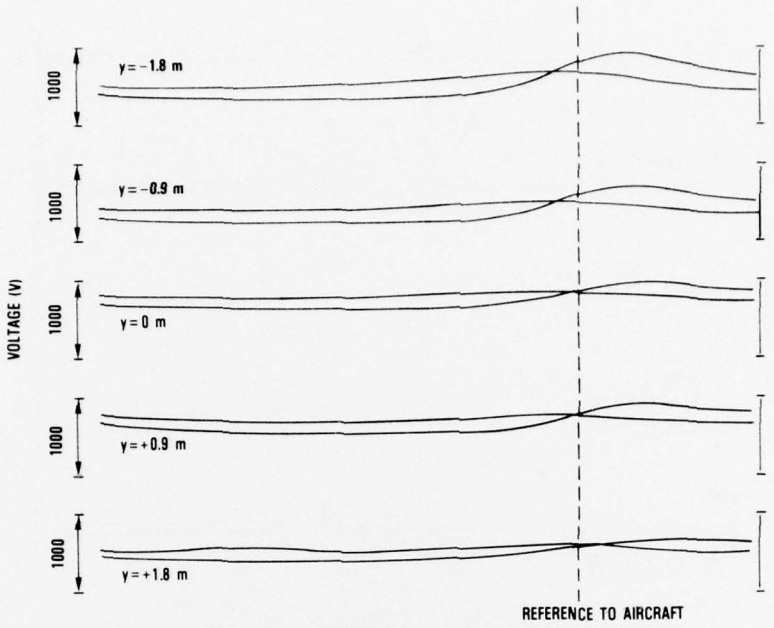

Figure C-40. Potential-difference plot for α = 120 deg, z = 2.7 m.

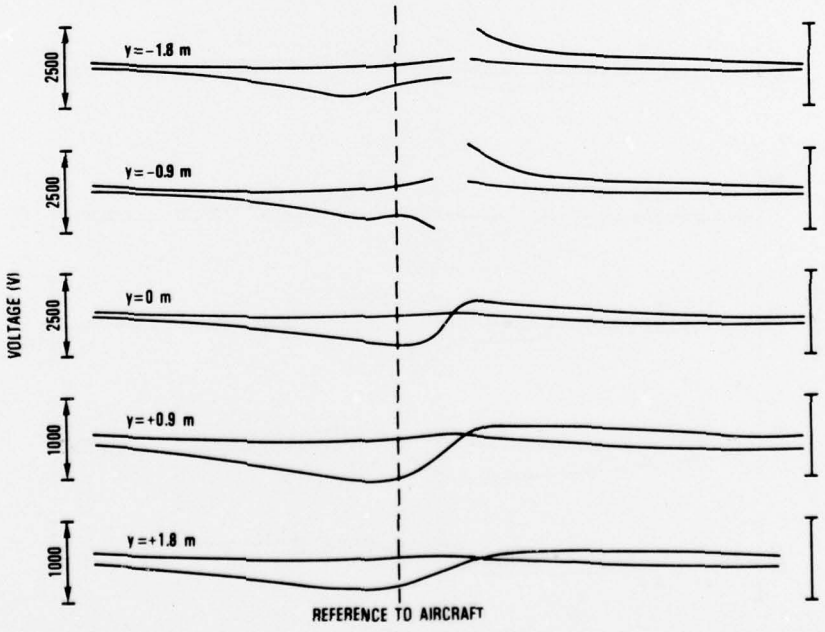

Figure C-41. Potential-difference plot for β = 30 deg, z = 0 m.

APPENDIX C

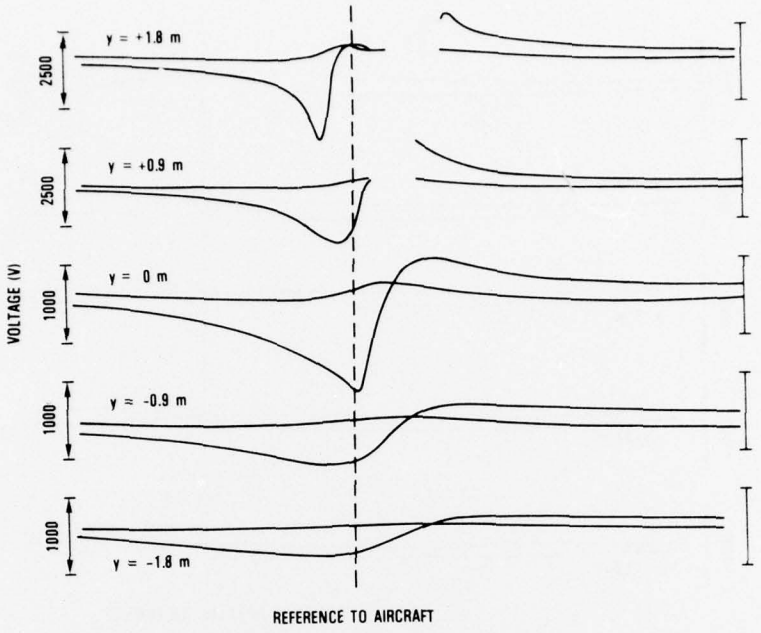

Figure C-42. Potential-difference plot for β = 30 deg, z = 0.9 m.

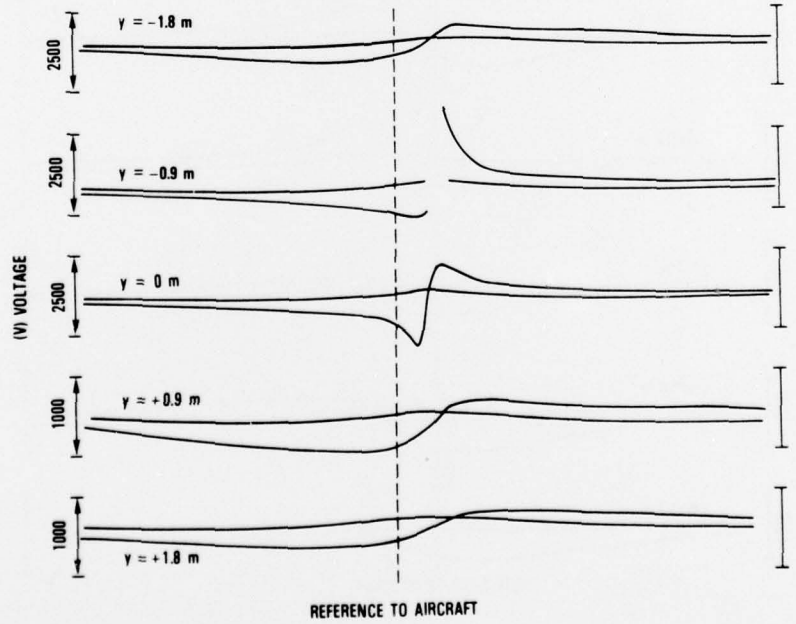

Figure C-43. Potential-difference plot for β = 30 deg, z = 1.8 m.

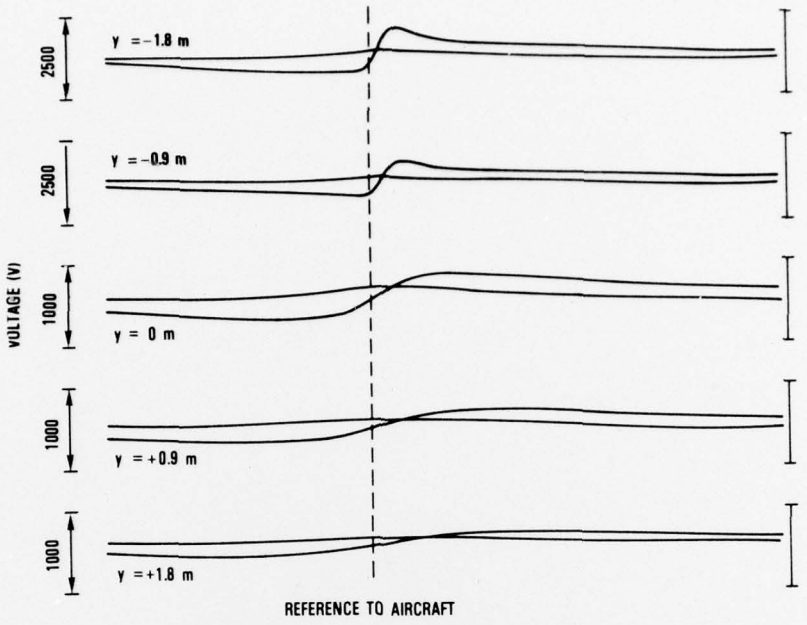

Figure C-44. Potential-difference plot for β = 30 deg, z = 2.7 m.

Preceding Page BLANK - NOT FILMED

DISTRIBUTION

DEFENSE DOCUMENTATION CENTER
CAMERON STATION, BUILDING 5
ALEXANDRIA, VA 22314
ATTN DDC-TCA (12 COPIES)

COMMANDER
USA RSCH & STD GP (EUR)
BOX 65
FPO NEW YORK 09510
ATTN LTC JAMES M. KENNEDY, JR.
CHIEF, PHYSICS & MATH BRANCH

COMMANDER
US ARMY MATERIEL DEVELOPMENT
& READINESS COMMAND
5001 EISENHOWER AVENUE
ALEXANDRIA, VA 22333
ATTN DRXAM-TL, HQ TECH LIBRARY

COMMANDER
US ARMY ARMAMENT MATERIEL
READINESS COMMAND
ROCK ISLAND ARSENAL
ROCK ISLAND, IL 61201
ATTN DRSAR-ASF, FUZE & MUNITIONS SPT DIV

COMMANDER
USA MISSILE & MUNITIONS CENTER & SCHOOL
REDSTONE ARSENAL, AL 35809
ATTN ATSK-CTD-F

ARMY RESEARCH OFFICE (DURHAM)
P.O. BOX 12211
RESEARCH TRIANGEL PARK, NC 27709
ATTN TECH LIBRARY

COMMANDER
FRANKFORD ARSENAL
BRIDGE & TACONY STREETS
PHILADELPHIA, PA 19137
ATTN N6000, AIR DEF & AIRCRAFT
WEAPONS DIV

COMMANDER
NAVAL AIR SYSTEMS COMMAND HQ
DEPT OF THE NAVY
WASHINGTON, DC 20360
ATTN NAIR-4135, MISSILES, WEAPONS
& EQUIP BR
ATTN NAIR-5323, WEAPONS DEV BR

COMMANDER
NAVAL ELECTRONIC SYSTEMS COMMAND
WASHINGTON, DC 20360
ATTN 350, ELECTRONIC &
SPECIAL WARFARE DIV

COMMANDER
NAVAL SURFACE WEAPONS CENTER
WHITE OAK, MD 20910
ATTN WA-05, FUZE PROGRAM MANAGER
ATTN WA-33, FUZING BR
ATTN WU-32, ELECTRICAL WEAPONS BR

COMMANDER
NAVAL WEAPONS CENTER
CHINA LAKE, CA 93555
ATTN CODE 30, SYSTEMS DEVELOPMENT DEPT
ATTN CODE 50, FUZE DEPT
ATTN CODE 533, TECHNICAL LIBRARY

COMMANDER
ARMAMENT DEVELOPMENT & TEST CENTER
EGLIN AFB, FL 32542
ATTN SD, DEP FOR ARMAMENT SYS
ATTN SD3, MUNITIONS SYS PROG OFFICE
ATTN DLJ, MUNITIONS DIV

DIRECTOR
AF AVIONICS LABORATORY
WRIGHT-PATTERSON AFB, OH 45433
ATTN WR, ELECTRONIC WARFARE DIV

HARRY DIAMOND LABORATORIES
ATTN LOWREY, AUSTIN, III, COL, COMMANDER/
FLYER, I.N./LANDIS, P.E./
SOMMER, H./OSWALD, R. B.
ATTN CARTER, W.W., DR., TECHNICAL
DIRECTOR/MARCUS, S.M.
ATTN KIMMEL, S., PAO
ATTN CHIEF, 0021
ATTN CHIEF, 0022
ATTN CHIEF, LAB 100
ATTN CHIEF, LAB 200
ATTN CHIEF, LAB 300
ATTN CHIEF, LAB 400
ATTN CHIEF, LAB 500
ATTN CHIEF, LAB 600
ATTN CHIEF, DIV 700
ATTN CHIEF, DIV 800
ATTN CHIEF, LAB 900
ATTN CHIEF, LAB 1000
ATTN RECORD COPY, BR 041
ATTN HDL LIBRARY (5 COPIES)
ATTN CHAIRMAN, EDITORIAL COMMITTEE
ATTN CHIEF, 047
ATTN TECH REPORTS, 013
ATTN PATENT LAW BRANCH, 071
ATTN GIDEP OFFICE, 741
ATTN LANHAM, C., 0021
ATTN CHIEF, 120
ATTN CHIEF, 140
ATTN STANN, B., 120
ATTN ARSEM, C., 120
ATTN CLASEN, S., 120
ATTN PARKHURST, R., 640
ATTN HARRISON, E., 160
ATTN WILKIN, N. D., (10 COPIES)

DEPARTMENT OF THE ARMY
HARRY DIAMOND LABORATORIES
2800 POWDER MILL RD
ADELPHI. MD 20783

OFFICIAL BUSINESS
PENALTY FOR PRIVATE USE $300

AN EQUAL OPPORTUNITY EMPLOYER

POSTAGE AND FEES PAID
DEPARTMENT OF THE ARMY
DOD 314

THIRD CLASS